Journal of Marine Research, 59, 355–390, 2001

Salt fingers in an unbounded thermocline

by Melvin E. Stern[1], Timour Radko[1,2] and Julian Simeonov[1]

ABSTRACT

Numerical solutions for salt fingers in an unbounded thermocline with uniform overall vertical temperature-salinity gradients are obtained from the Navier-Stokes-Boussinesq equations in a finite computational domain with periodic boundary conditions on the velocity. First we extend previous two-dimensional (2D) heat-salt calculations [Prandtl number $Pr = \nu/k_T = 7$ and molecular diffusivity ratio $\tau = k_S/k_T = 0.01$] for density ratio $R = 2$; as R decreases we show that the average heat and salt fluxes increase rapidly. Then three-dimensional (3D) calculations for $R = 2.0$, $Pr = 7$, and the numerically "accessible" values of $\tau = 1/6, 1/12$ show that the ratio of these 3D fluxes to the corresponding 2D values [at the same (τ, R, Pr)] is approximately two. This ratio is then extrapolated to $\tau = 0.01$ and multiplied by the directly computed 2D fluxes to obtain a first estimate for the 3D heat-salt fluxes, and for the eddy salt diffusivity (defined in terms of the overall vertical salinity gradient).

Since these calculations are for relatively "small domains" [$O(10)$ finger pairs], we then consider much larger scales, such as will include a slowly varying internal gravity wave. An analytic theory which assumes that the finger flux is given parametrically by the small domain flux laws shows that if a critical number A is exceeded, the wave-strain modulates the finger flux divergence in a way which amplifies the wave. This linear theoretical result is confirmed, and the finite amplitude of the wave is obtained, in a 2D numerical calculation which resolves both waves and fingers. For highly supercritical A (small R) it is shown that the temporally increasing wave shear does *not* reduce the fluxes until the wave Richardson number drops to $\sim$0.5, whereupon the wave starts to overturn. The onset of density inversions suggests that at later time (not calculated), and in a sufficiently large 3D domain, strong convective turbulence will occur in patches.

1. Introduction

The early experimental and theoretical investigations of double-diffusive convection (e.g., Linden, 1973, 1978; Kunze, 2000; Radko and Stern, 2000) considered a relatively *thin* salt finger layer sandwiched between two very deep mixed layers with specified temperature (ΔT_*) and salinity (ΔS_*) *differences;* analogous quantities are used in (isothermal) sugar-salt experiments, where "T_*" refers to the substance of higher molecular diffusivity (k_T) and "S_*" refers to the lower diffusivity $k_S < k_T$. The experimental laws

1. Department of Oceanography, The Florida State University, Tallahassee, Florida, 32306-4320, U.S.A. ***email: stern@ocean.fsu.edu***

2. Present address: Department of Earth, Atmospheric and Planetary Sciences, Massachusetts Institute of Technology, Cambridge, Massachusetts, 02139, U.S.A. ***email: timour@ocean.mit.edu***

relating the vertical heat/salt flux to $(\Delta T_*, \Delta S_*)$ were thought to be applicable to the relatively strong vertical temperature gradient region observed in steplike ("staircase") profiles in the ocean thermocline, but oftentimes the thickness of these gradient regions greatly exceeded the (scaled) laboratory values. In this case the fluxes should be related to the observed vertical *gradients* $\partial \bar{T}_*/\partial z_*$, $\partial \bar{S}/\partial z_*$. As indicated below, Shen (1995) has made a start on the numerical problem; also see Kunze (1987) for a much simpler *ad hoc* theory.

An important physical difference between the thick and thin layer regimes arises because the fingers in the latter case (Radko and Stern, 2000) are coherent over the entire extent of the gradient layer and are thereby able to reduce its mean vertical S_*-gradient toward a state of marginal stability; this is a well-known mechanism for offsetting the linear growth rate of a normal mode and equilibrating its amplitude. The equilibration mechanism is quite different in the "thick" regime since the fingers are vertically coherent only over a small fraction of the average height $L_z \to \infty$ of the gradient region. Consequently, these fingers do not alter the "overall" gradients $(\partial \bar{T}_*/\partial z_*, \partial \bar{S}/\partial z_*)$, in the unbounded model, although they do alter the horizontal (x_*, y_*) average at each z_* and each time (t_*). If the density ratio R is not too small, the statistically steady state consists of a "pure" finger field in which amplitude equilibration occurs by transfer of energy to other wavelengths; i.e., classical "triad" interactions [see the unbounded sugar-salt calculations of Radko and Stern (1999)].

Shen (1995) has made an unbounded domain calculation in *two* dimensions (2D) for heat-salt [$Pr = 7$, $\tau = 0.01$] fingers with $R = 2.0$. Starting from rest, the sequence of primary and secondary instabilities (Holyer, 1981, 1984) eventually lead to a statistical steady state with average heat/salt fluxes (F_{T*}/F_{S*}). Shen's work will be extended in three respects; first we obtain (Section 3) the 2D flux gradient laws for other values of R. Such variability occurs in the ocean on a vertical scale of a couple of meters and in connection with isopycnal intrusions [cf. Ruddick *et al.,* 1999] between water masses with different T-S properties. Next we need to determine (Section 4) whether the 3D fluxes are significantly larger or smaller than in 2D. For the case of sugar-salt ($\tau = 1/3$) gradients, Radko and Stern (1999) showed that the 2D fingers are unstable, and the resulting 3D fingers have much larger fluxes. A 3D heat/salt calculation at $R = 2$ for $\tau \simeq 0.01$ is, however, not feasible because of the smallness of the salinity dissipation scale, and therefore an indirect method (viz., extrapolation from numerically accessible values of $\tau \ll 1$) is used (Section 4) to obtain a first estimate of the 3D heat-salt flux at $R = 2$.

All the foregoing calculations are for a small computational domain [$O(10)$ finger pairs], and, therefore, in our third problem the domain size is increased by an order of magnitude. This allows us to consider (Section 5) the coupling of a slowly varying internal gravity wave with the finger flux. The effect of the latter is parameterized by the previously calculated "small domain" laws. Although the procedure is similar to frequently used eddy coefficient formalisms (e.g., Schmitt, 1981; Walsh and Ruddick, 1995), these lack the quantitative knowledge of the relevant coefficients, such as is supplied by Sections 3 and 4.

The predicted (Section 5) amplification of the internal wave is then confirmed by a 2D numerical calculation (Section 6) which resolves both fingers and large-scale wave. The discussion in Section 7 shows that the amplified internal wave can overturn if $R - 1$ is small.

The results of the three interrelated parts (Section 3, Section 4 and Sections 5–7) are summarized in Section 8, along with a reference to relevant measurements in the open ocean.

2. The nondimensional Navier-Stokes-Boussinesq equations

As is conventional, the expansion coefficients (α, β) relating temperature and salinity (T_*, S_*) to the density (ρ_*) will be absorbed in a new "temperature" αT_* and "salinity" βS_*; likewise for the new average convective fluxes $F_T = \alpha F_{T*}$, $F_S = \beta F_{S*}$. The density ratio is $R = (\alpha \partial \bar{T}_*/\partial z_*)/(\beta \partial \bar{S}_*/\partial z_*)$, the average heat flux is given by a Nusselt number Nu:

$$Nu = \alpha F_{T_*} (\alpha \partial \bar{T}_*/\partial z_*)^{-1} k_T^{-1},$$

and the heat/salt flux ratio is given by

$$\gamma = \alpha F_{T_*}/\beta F_{S_*} = F_T/F_S.$$

Note that (by definition) the *overall* vertical T_*, S_* gradients in a given computational domain are constants independent of the motion generated, even if a staircase thermocline with large steps (Kelley, 1984) should develop; the only relevant nondimensional parameters are (Pr, R, τ) and the (large) nondimensional domain size. Also note that there is no basic shear or horizontal T_*, S_* gradient in the model.

Also conventional (e.g., Radko and Stern, 1999) is the nondimensionalization of the Navier-Stokes Boussinesq equations (2.1) using the length scale $d = (\nu k_T/(g\alpha \partial \bar{T}_*/\partial z_*))^{1/4}$, the velocity scale k_T/d, the time scale $d^2 k_T$, the pressure scale $\nu k_T/d^2$, and $\alpha d(\partial \bar{T}_*/\partial z_*)$ as the scale for the *deviations* (T/S) from the undisturbed temperature/salinity. This scaling makes the buoyancy force in Eq. 2.1 of the same order as the viscous force and the pressure force. The nondimensional heat/salt equations (2.1c), (2.1d) are expressed in terms of the departures ($T = T' + \theta$ and $S = S' + \sigma$) of the total temperature/salinity from the undisturbed fields, where $\theta(z, t)$, $\sigma(z, t)$ are the horizontal averages of T, S. These nondimensional Boussinesq equations are

$$\begin{cases} Pr^{-1} d\mathbf{v}/dt = -\nabla p + \nabla^2 \mathbf{v} + (T' - S')\mathbf{k}, & (2.1a) \\ \nabla \cdot \mathbf{v} = 0, & (2.1b) \\ \dfrac{d}{dt}[T' + \theta] + w = \nabla^2 (T' + \theta), \qquad T \equiv T' + \theta & (2.1c) \\ \dfrac{d}{dt}[S' + \sigma] + \dfrac{1}{R} w = \tau \nabla^2 (S' + \sigma), \qquad S \equiv S' + \sigma. & (2.1d) \end{cases}$$

Note that the undisturbed temperature gradient appears explicitly in the coefficient [unity] of the w term in (2.1c), and in the undisturbed salinity gradient $1/R$. Also note that two more (mean-field) equations for $\partial\theta/\partial t$, $\partial\sigma/\partial t$ are implicit in (2.1c,d), and will appear as the zero horizontal wave number component in the Fourier series calculations given below. Eqs. (2.1) will be solved for periodic boundary conditions on $\mathbf{v}$, T, S in a rectangular domain of size (L_x, L_y, L_z). In the statistically steady case, Eq. (2.1c) yields the "power integral."

$$-\langle\overline{wT}\rangle_{av} = \langle(\overline{\nabla T})^2\rangle_{av} \tag{2.1e}$$

where "bar," "brace," "av" indicate horizontal, vertical, and time average, respectively. Note that although the following calculations focus on (Nu, γ) the important r.m.s. temperature gradient is immediately given by Eq. (2.1e). Since F_{T_*} is the average of $(k_T/d)w(d\partial\bar{T}_*/\partial z_*)T$ the value of Nu is

$$Nu = -\langle\overline{wT}\rangle_{av} \tag{2.1f}$$

and the "Cox number" $\langle(\overline{\nabla T})^2\rangle_{av}$ is equal to Nu. The power integral obtained from (2.1a) gives a time rate of increase of "kinetic energy" $\langle\mathbf{v}^2\rangle Pr^{-1}/2$ equal to the buoyancy work minus the dissipation.

Eqs. (2.1) will be integrated using a pseudo-spectral method in which all the equations are inverted exactly in the Fourier space, and the aliasing error is removed by zero padding. Time integration is performed by a fourth order Runge-Kutta scheme [with the integrating factor technique], and a periodic Cartesian grid with (N_x, N_y, N_z) points is used to compute the nonlinear terms. The code is essentially the same as in Radko and Stern (1999). Extensive tests of the adequacy of the grid point resolution, domain size, and time step Δt have been made; for example see Eq. (3.1), Figure 13b, Sec 4 (¶2), Figure 14 discussion, and Figure 12.

3. 2D fluxes for $Pr = 7$, $\tau \leq 0.01$

Our final estimate (Section 4) of the 3D heat/salt fluxes [for fixed $R = 2$, $Pr = 7$] will require information about the asymptotic ($\tau \ll 1$) behavior of the solutions of Eqs. 2.1, and, therefore, we will start the required sequence of calculations with $\tau = 1/6$, in a 2D computational domain whose horizontal width contains four fastest growing wavelengths (F.G.W.) with $\mu \equiv$ (F.G.W.)/(longest finite z-wavelength) $= 0.1$, (64×128 grid). Figure 1a shows the temporal variation of the x-z averaged ($-wT$), and although the salt flux was computed it is not shown. The time averages are $Nu = 12 \pm 2$, $\gamma = 0.75$. Essentially the same $Nu = 12 \pm 3$, $\gamma = 0.73$ was obtained (not shown) for a smaller $\mu = 1/20$ (64×256 grid). A discussion of the corresponding flux for 3D fingers (Fig. 1b) is deferred to Section 4, and we now continue the discussion of the 2D calculations. Figure 1c shows the decreased flux which occurs for $\tau = 1/6$ when R is increased to $R = 2.5$. For a

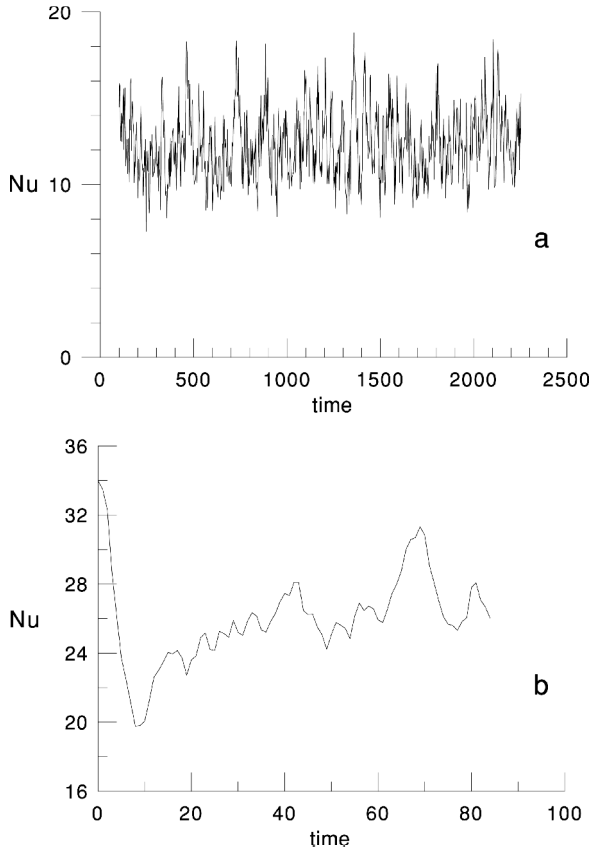

Figure 1. Comparison of 2D/3D fluxes. (a) The 2D nondimensional heat flux is plotted as a function of time for $Pr = 7$, $R = 2$, $\tau = 1/6$ with four F.G.W. and 16 points/finger pair (see text). The time origin is of no significance since initialization was obtained using the output of a previous test run. (b) The corresponding 3D calculation as discussed in Section 4. (c) Same 2D calculation as in (a) except $R = 2.5$. (d) Same as (c) except for 3D. (e) Same 2D calculation as in (a) except for $\tau = 1/12$. (f) Same as (e) except for 3D (128^3 grid). In all cases the 3D fluxes exceed the corresponding 2D values by at least a factor of two.

smaller $\tau = 1/12$ at $R = 2.0$, Figure 1e shows that the heat flux increases slightly compared to Figure 1a. The time averages for even smaller τ (at $R = 2$) are:

$$\begin{aligned}
&\tau = 1/12,\ Nu = 13.5 \pm 2,\ \gamma = 0.66 \pm 0.05,\ 4\ \text{F.G.W.}(64 \times 128)\\
&\tau = 1/24,\ Nu = 19 \pm 3,\ \gamma = 0.63 \pm 0.04,\ 4\ \text{F.G.W.}(128 \times 256)\\
&\tau = 1/24,\ Nu = 19 \pm 2,\ \gamma = 0.63 \pm 0.03,\ 16\ \text{F.G.W.}(512 \times 256) \qquad (3.1)\\
&\tau = 1/48,\ Nu = 19 \pm 3,\ \gamma = 0.58 \pm 0.04,\ 4\ \text{F.G.W.}(256 \times 512)\\
&\tau = 1/96,\ Nu = 22 \pm 3,\ \gamma = 0.57 \pm 0.04,\ 4\ \text{F.G.W.}(256 \times 512)
\end{aligned}$$

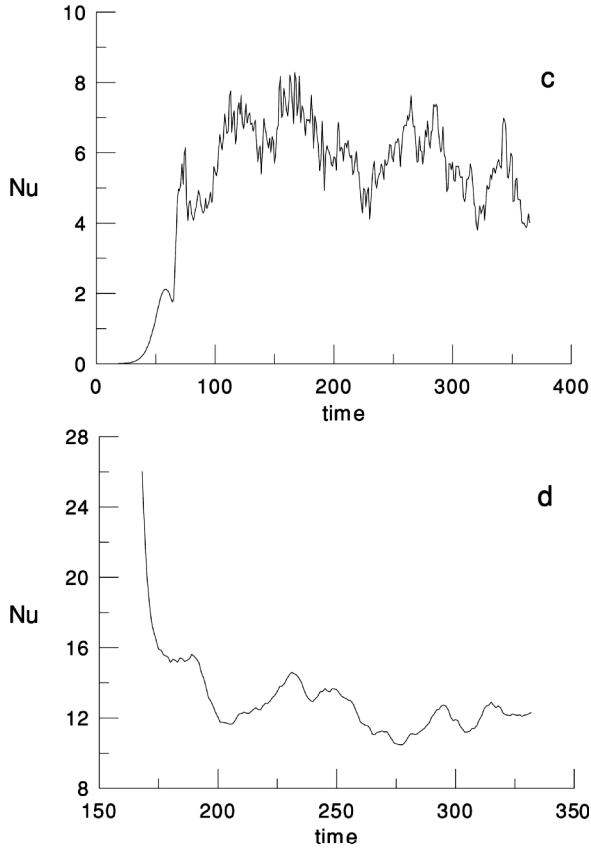

Figure 1. (Continued)

The last run agrees with Shen's (1995) result for $R = 2.0$, $\tau = 0.01$: $Nu = 20$, $\gamma = 0.61$, $L_x = 8$ F.G.W. Eqs. (3.1) indicate that as τ decreases from $\tau = 1/12$ to $\tau = 0.01$, Nu increases and γ decreases toward asymptotic values, which are given (with sufficient accuracy for present purposes) by the values at $\tau = 1/24$.

The plot of *total* density (including the basic gradient) for $\tau = 1/24$ (Fig. 2) reveals the chaotic nature of the fingers, and provides insight into the life cycle of an individual salt finger. In the earliest (top, right) of the four stages shown in Figure 2c we isolated a relatively small amplitude density anomaly which is completely surrounded by less dense fluid (not shown). The plume is descending and increasing its maximum density (due to the lateral heat exchange) in the second and third stages. In the fourth stage the plume (laterally offset) reaches a stagnation level (zero vertical velocity) where it spreads laterally and then tends to rise in a neighboring upgoing finger. Subsequently the "identity" of the plume will be lost, so that the vertical distance λ between the first and last stages [i.e., $O(10)$ finger

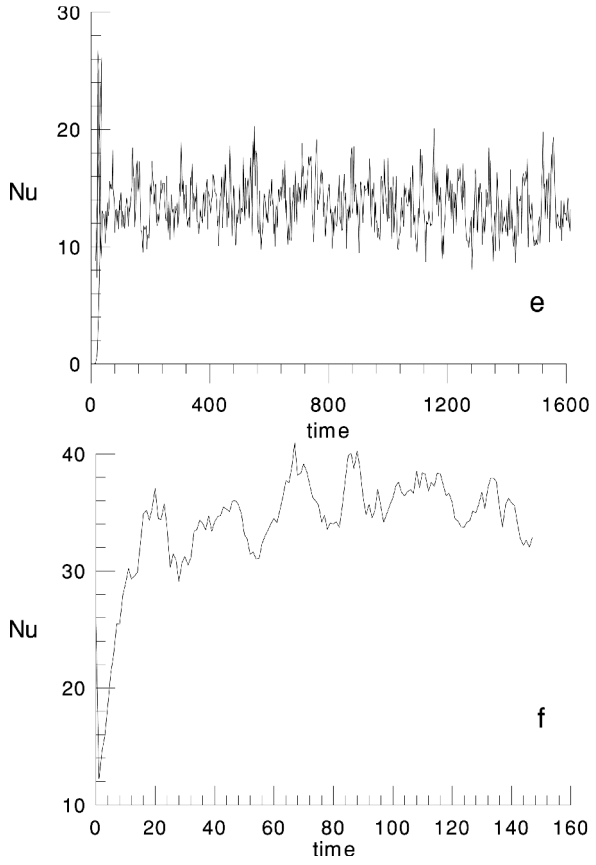

Figure 1. (Continued)

wavelengths] may be designated as a vertical "mixing length." It is conjectured that in the *three*-dimensional case (Section 4), there will be a greater probability that some of the fluid surrounding a stagnation point contains a down-going finger which enables the laterally spreading plume (Fig. 2c) to *continue* downward, thereby increasing λ. This suggests that in 3D the r.m.s. T/S anomalies and the heat/salt flux will be larger than in 2D. This argument does not apply to the "thin" finger layer case (Linden, 1974) where the plume descends monotonically.

Before turning to the 3D problem, it is important to indicate how the 2D fluxes for $\tau = 1/24$ vary with R. Figure 3a gives the temporal variation of heat flux for $R = 1.25$, and Figure 3b shows that the time average flux is five times larger than for $R = 2$. Note that as R decreases, the eddy salt diffusivity [which will be seen (Section 6) to be proportional to $R\ Nu/\gamma$] also increases, in contrast to the result of oversimplified calculations (Kunze, 1987).

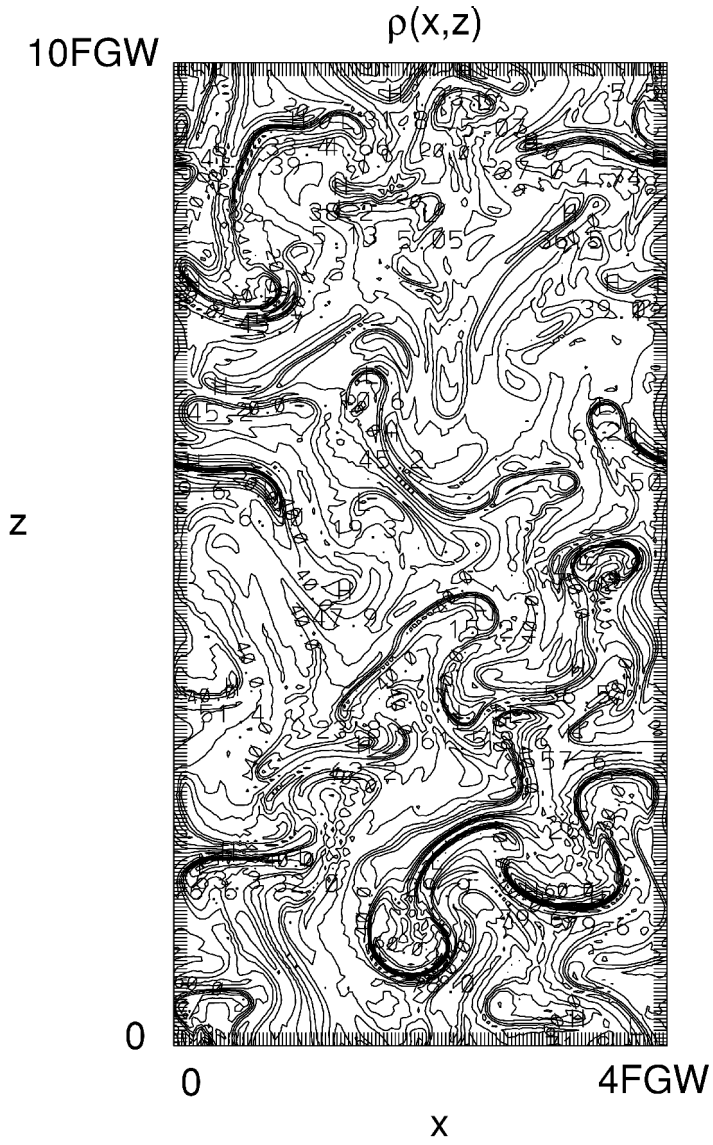

Figure 2. The chaotic structure and large gradients in fingers. (a) Isolines of constant *total* density ρ in the entire domain for 2D fingers at $\tau = 1/24$, $R = 2$, $Pr = 7$ (see text). (b) The nominal density is divided into three parts, the first prints only the lowest (0–25) isopycnals; the middle diagram prints the (25–45) range; and the last prints only the largest range. (c) A temporal sequence of a "finger" obtained by printing only the isopycnals in a very restricted density and spatial interval. The last snapshot is laterally offset to avoid overlapping with the three earlier ones. Note the limited vertical extent and "life history" of a plume, and its tendency to rise after the stagnation point is reached. The total elapsed time is 4.5 nondimensional units.

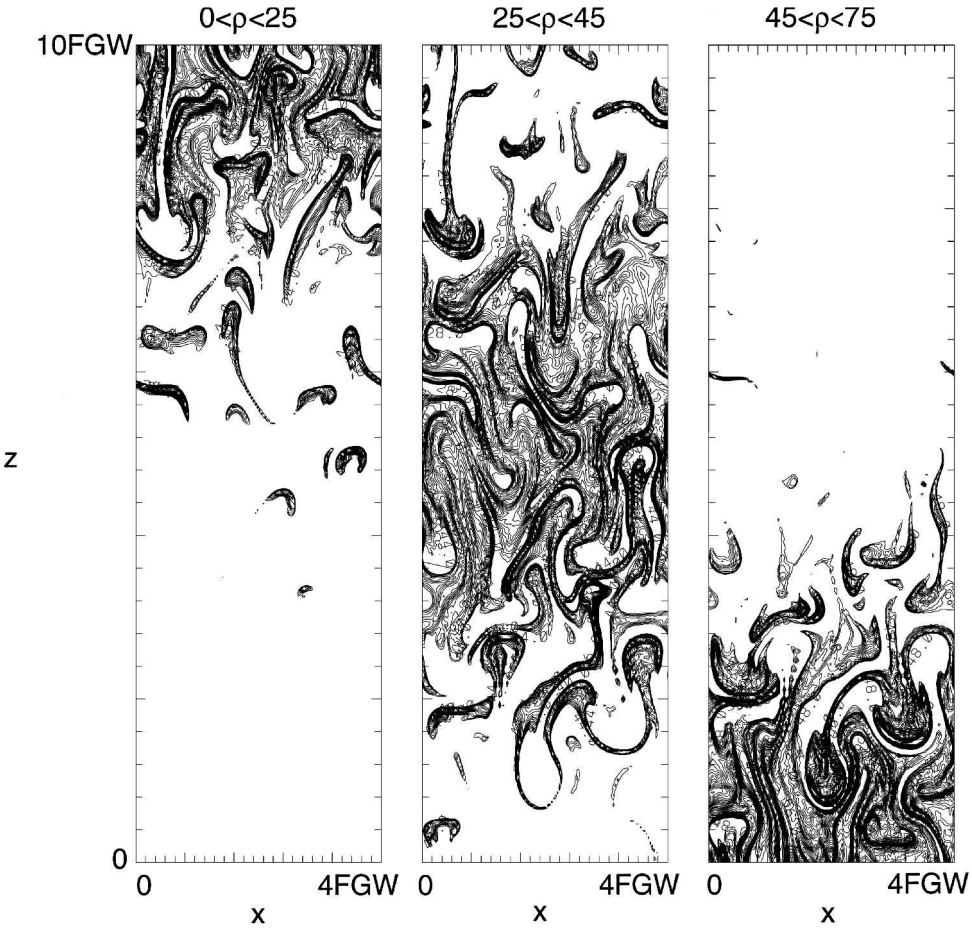

Figure 2. (Continued)

4. 3 D fluxes for $Pr = 7$

Since the 2D fluxes (Eq. 3.1) asymptote as $\tau \to 0.01$ it is plausible that the ratio

$$\frac{\text{3D-heat flux}}{\text{2D-heat flux}} \tag{4.1}$$

asymptotes, or at least varies slowly in the vicinity of $\tau = 0.01$. We, therefore, propose to compute (4.1) at numerically "accessible" values of $\tau > 0.01$, and to extrapolate the ratio to $\tau = 0.01$; the result will then be multiplied by the computed (Eq. 3.1) 2D-flux at $\tau = 0.01$ to obtain a first estimate of the 3D flux for the heat-salt case.

A 3D-calculation was first made for $\tau = 1/6$ in a rather small domain containing only 2×2 F.G.W. in the horizontal (each F.G.W. is $9.05\boldsymbol{d}$) with $\mu = 0.1$ and $32 \times 32 \times 64$ grid points. The initial condition consisted of a normal mode (of the linear problem) whose

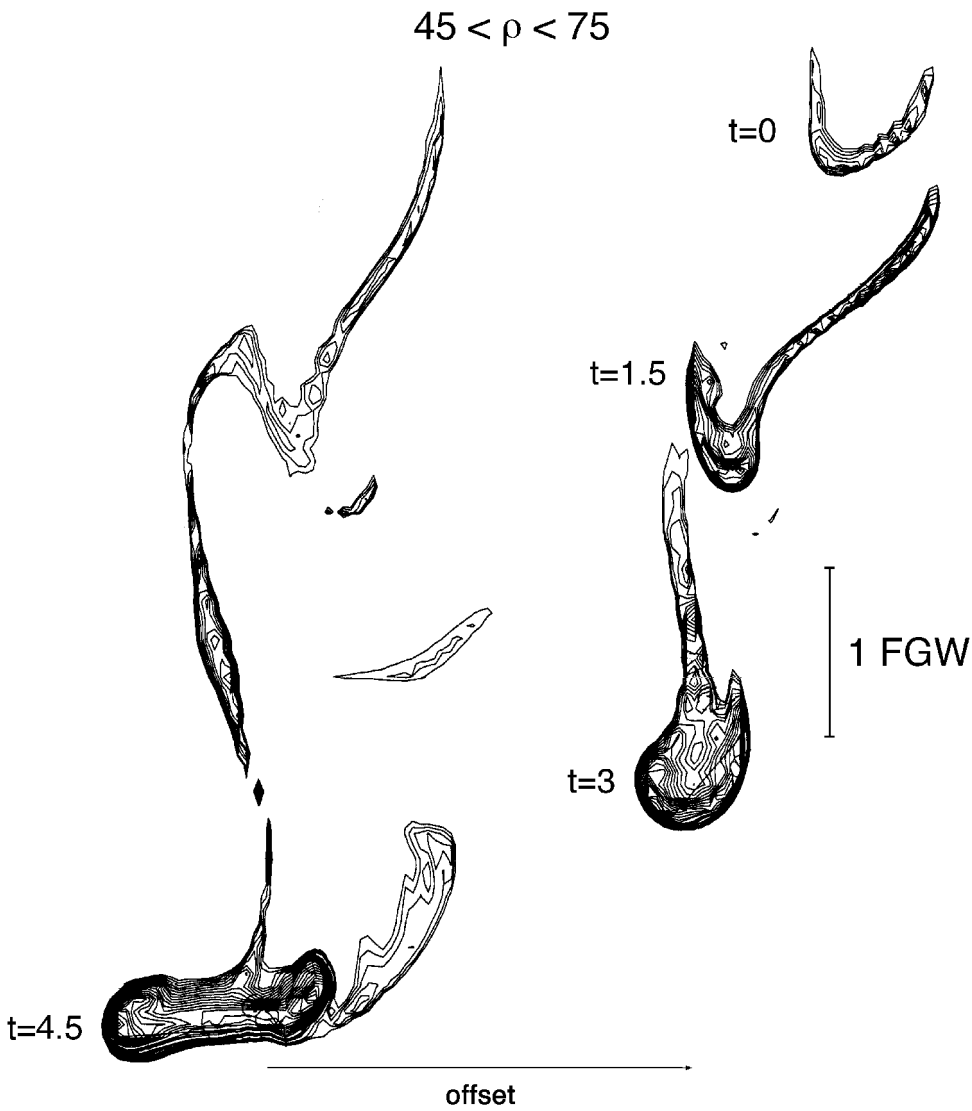

Figure 2. (Continued)

horizontal wave length equaled one F.G.W., and whose vertical wavelength corresponded to μ (vertical wavenumber zero is present in the computer noise). In the subsequent evolution of this normal mode the exponential increase in amplitude agreed with linear theory, and eventually flux equilibration occurred with oscillations about $Nu = 28 \pm 5$, $\gamma = 0.67 \pm 0.05$. The adequacy of the time step was confirmed by the balance (to 0.7%) of the terms in the equation for the production/dissipation of T-variances, but inadequate resolution of the smallest S-wavelengths was apparent in the ∇S spectrum, which dropped

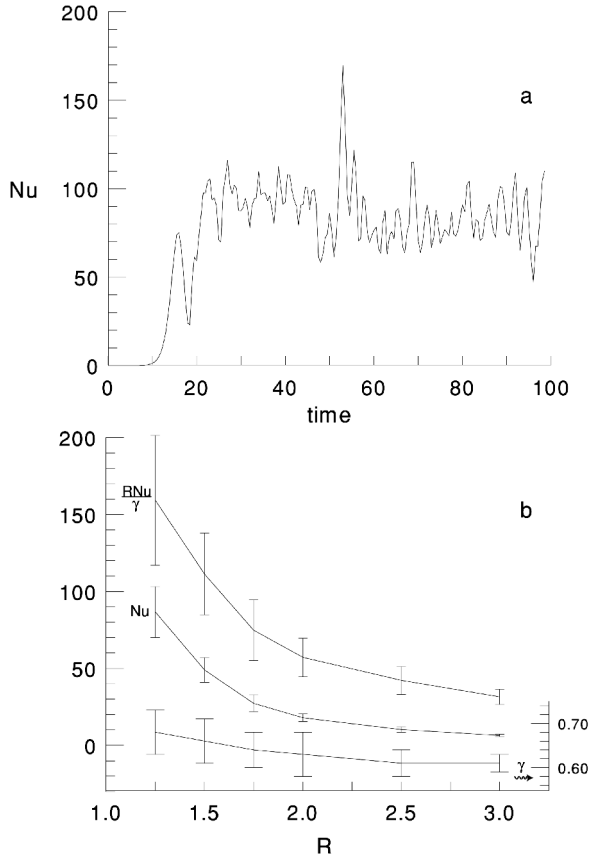

Figure 3. 2D heat-salt fluxes for various R (using $\tau = 1/24$). (a) The time variation of heat flux when $R = 1.25$. (b) The variation of Nu, γ. The third curve is proportional to the eddy salt diffusivity $[Rk_T(Nu/\gamma)]$. The vertical bars indicate the r.m.s. temporal deviation. A curve which fits the heat-flux is $Nu = 1.06 \exp(5.62/R)$.

precipitously to zero at the smallest zero padded vertical wave number m. Therefore, the vertical resolution was doubled and the calculation was continued. Although this only resulted in a small increase in the flux to $Nu = 31 \pm 5$, the tail of the ∇S spectrum at large m behaved more satisfactorily by tapering off more gradually to zero; this suggests that the fluxes are insensitive to the smallest ∇S scale. Figure 4 shows typical salinity and vertical velocity sections for this run. To obtain our final result for the fluxes at $\tau = 1/6$ (Fig. 1b) the number of finger pairs in x and y was doubled, yielding average values $Nu = 26 \pm 3$, $\gamma = 0.68$; this Nu is only 15% smaller than the previous run with less fingers.

Comparison of Figures 1a,b gives the ratio

$$\frac{\text{3D-heat flux}}{\text{2D-heat flux}} \simeq \frac{26}{12} = 2.2 \ @ \ \tau = \frac{1}{6}, R = 2. \tag{4.2}$$

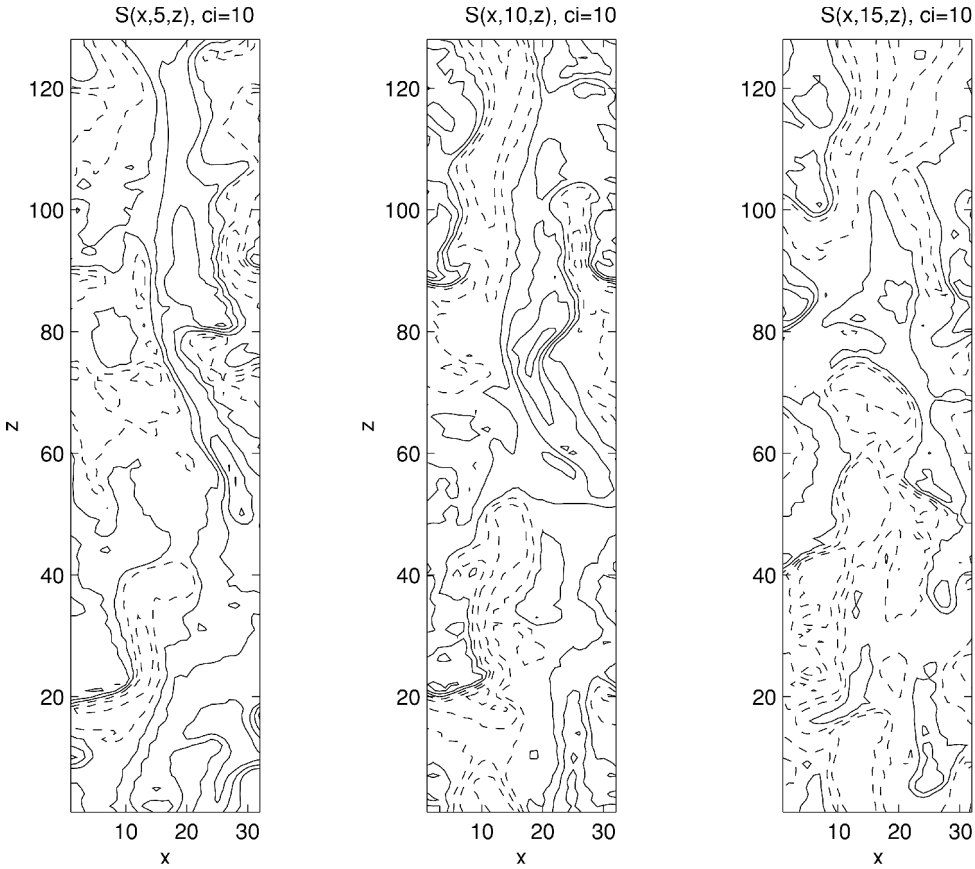

Figure 4. An example of the 3D calculations for $Pr = 7$, $R = 2$, $\tau = 1/6$; there are $2 \times 2 \times 10$ F.G.W. (see text). (a) The value of S at various y. (b) Horizontal S sections at various z. (c) Horizontal sections of vertical velocity. The solid lines are ≥ 0. Contours are separated by "ci" units. The units along the axis are in grid point numbers. There is no vertical exaggeration.

A similar 3D calculation for $R = 2.5$ is shown in Figure 1d, and comparison with Figure 1c yields approximately the same (3D)/(2D) flux ratio as in Eq. 4.2. To confirm the approach to the τ-asymptote of the ratio in (4.2) a 3D calculation at $R = 2.0$ was made for $\tau = 1/12$ (on a super-computer). Initialization was provided by the last output of the $\tau = 1/6$ run, and the horizontal grid spacings were halved. Figure 1f shows the spatially averaged heat flux with time average $Nu = 35 \pm 3$, and $\gamma = 0.63$. The ratio of this Nu to the corresponding 2D flux (Fig. 1e, Eq. 3.1) at the same $\tau = 1/12$ is

$$\frac{\text{3D-heat flux}}{\text{2D-heat flux}} \simeq \frac{35}{14} = 2.5 \; @ \; \tau = \frac{1}{12}, R = 2. \tag{4.3}$$

Thus we see that halving τ only *increases* Eq. 4.2 by 0.3 (or 10%), and this justifies an extrapolation to the heat-salt case, for which the estimate is

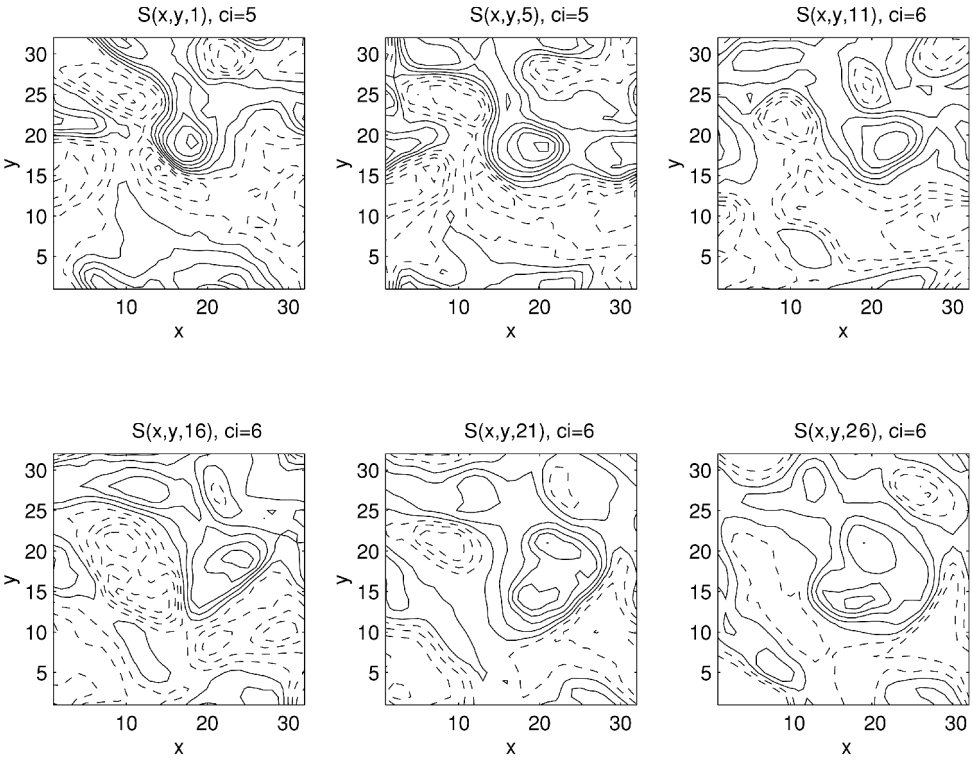

Figure 4. (Continued)

$$\frac{\text{3D-heat flux}}{\text{2D-heat-flux}} = 2.5 \pm 0.3 \ @ \ \tau = 0.01, R = 2. \tag{4.4}$$

To obtain a first approximation for the 3-D value of Nu for *heat-salt* at $R = 2$, the ratio in Eq. (4.4) is multiplied by the previously calculated [Eq. 3.1] 2D value of $Nu \cong 20$ to get

$$Nu = 20(2.5) \simeq 50 \quad (R = 2,\ Pr = 7,\ \tau = 0.01)$$

$$\gamma \simeq 0.63. \tag{4.5}$$

It is convenient to *define* an eddy salt diffusivity D_S by dividing the salt flux $(F_{T_*}/\beta\gamma)$ by the overall salinity gradient in the computational domain:

$$D_S \equiv \frac{F_{T_*}/\gamma}{\beta\partial\bar{S}_*/\partial z_*} = \frac{k_T Nu(\alpha\partial\bar{T}_*/\partial z_*)}{\gamma\beta\partial\bar{S}_*/\partial z_*} = \frac{k_T RNu}{\gamma} \tag{4.6}$$

$$D_S = \left[\frac{(1.5 \times 10^{-3}\ \text{cm}^2/\text{sec})(2.0)}{0.63}\right]50 = 0.24\ \text{cm}^2/\text{sec}, \tag{4.7}$$

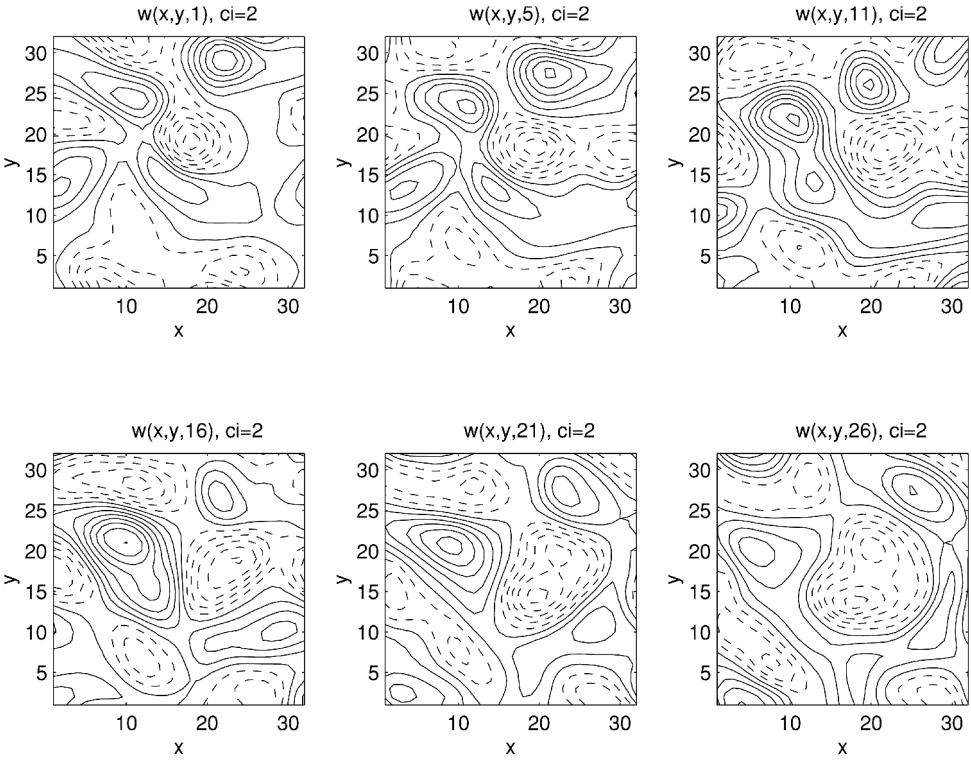

Figure 4. (Continued)

and a similar definition for the eddy heat diffusivity gives

$$D = \frac{\gamma D_S}{R} = 0.076 \text{ cm}^2/\text{sec}.$$

The variation of D_S with R for 2D-fingers is, therefore, proportional to the $(R/\gamma)\,Nu$ curve in Figure 3.

Ocean heat flux measurements (Sec. 8) based on Eq. (2.1e) assume that the right-hand side is partitioned equally between vertical r.m.s. gradients and horizontal ones. On the other hand our computed value of the r.m.s. $\partial T/\partial z$ for $R = 2$, $\tau = 1/12$ is

$$\frac{\langle(\overline{\partial T/\partial z})^2\rangle \text{av}}{\langle(\overline{\nabla T})^2\rangle \text{av}} = 0.18, \tag{4.8}$$

which is less than half that which would occur with equi-partition of ∇T in all three directions. From the order of magnitude of the inertial terms in these calculations we also found that the finger Reynolds number is of order unity (as expected). But as we shall now see the finger flux is capable of generating much larger Reynolds number motions.

5. Parametric theory of the collective instability of salt fingers

What happens when the domain size and the number of finger pairs increases by an order of magnitude? Consider a 3D stochastic field of fingers (e.g., Section 4) whose ensemble average is stationary and homogeneous (independent of x, y, z), with uniform average overall gradients, $\bar{T}_z(z)$, $\bar{S}_z(z)$, $R = \bar{T}_z/\bar{S}_z$. For the purpose of this section (only) it is convenient to start with *dimensional* coordinates, so that T, S are given here in buoyancy units. Assume that the small domain flux gradient laws [cf. Sections 3, 4] have been computed as a function of R [for any given τ, Pr], so that the dimensional downward convective fluxes are known and are given by

$$F_T = +k_T Nu\bar{T}_z \equiv +D\bar{T}_z, \tag{5.1a}$$

$$F_S = +\frac{R}{\gamma}k_T Nu\bar{S}_z = +\frac{R}{\gamma}D\bar{S}_z = D_S(R)\bar{S}_z, \tag{5.1b}$$

$$D \equiv k_T Nu,\ D_S = \frac{R}{\gamma}D. \tag{5.1c}$$

[The small molecular fluxes may easily be included in (5.1) if desired.]

Now subject this statistical equilibrium to (an ensemble average) perturbation whose z-wavelength $2\pi H$ is much larger than the dominant finger width, and whose x-wavelength $2\pi Hk^{-1}$ is even larger ($k \ll 1$). The ensemble average temperature, salinity, and velocity perturbation T'', S'', $\mathbf{U}''$ may (without loss of generality in the following linear theory) be taken as 2D, even if the finger field is 3D. In the absence of fingers this "large scale" perturbation would behave like a classical low-frequency internal gravity wave [damped mainly by viscosity, if $\nu \gg k_T \gg k_S$]. But in the presence of the fingers and their perturbed heat, salt and momentum flux divergences, there will be a slight modification of the internal wave due to several distinct physical effects. As in Stern's (1969) "collective instability" theory, the $\mathbf{U}''$-shear can differentially tilt different groups of fingers, thereby changing the *direction* of the convective heat flux vector in different regions of the large-scale motion; the resulting flux convergence then modifies the large-scale buoyancy force, causing an "overstable" amplification of a low-frequency ($k \ll 1$) internal wave. But that theory neglected the perturbation in the *magnitude* of the flux vectors, and it is this effect which is isolated below. Also previously neglected was the perturbed *momentum* flux vector, which can result in either an upgradient or a downgradient mean momentum flux; the latter is produced by finger plumes sinking or rising into regions with different $\mathbf{U}''$, whereas an upgradient flux can be produced by the shear-induced correlation of the vertical and horizontal finger velocities. The eddy momentum flux is neglected below and will be discussed in the Appendix; *all* effects will be included in the finite amplitude numerical calculation (Section 6).

We assume that the variations of F_T, F_S on the scale of the wave can be computed *parametrically* from (5.1) using the perturbed large-scale T_z, S_z gradients on the same

scale. The validity of this (rather conventional eddy coefficient parameterization) depends on the fact that the wave field varies so slowly in space-time that each region, containing a large number of fingers, has time to adjust to the statistical equilibrium flux corresponding to the local gradients. The large-scale finger flux convergences $(+\partial F_T/\partial z,\ +\partial F_S/\partial z)$ will subsequently be set equal to $\partial/\partial t(T'', S'') + w''(\bar{T}_z, \bar{S}_z)$, where w'' is the vertical component of U'', to obtain the modified density force in the wave.

We must take into account that F_T depends on both the temperature gradient and on the density ratio, whose perturbed value is $R = (\bar{T}_z + T''_z)/(\bar{S}_z + S''_z)$; and whose infinitesimal deviation from $\bar{R} = \bar{T}_z/\bar{S}_z$ is

$$R'' = \frac{\bar{T}_z + T''_z}{\bar{S}_z + S''_z} - \frac{\bar{T}_z}{\bar{S}_z} = \bar{R}\left(\frac{T''_z}{\bar{T}_z} - \frac{S''_z}{\bar{S}_z}\right). \tag{5.1d}$$

These fluctuations in density ratio are due to the finger heat/salt flux, for otherwise a pure gravity wave would cause the bracketed term to vanish. The first order expansions of the fluxes $F_T = +D(R)[\bar{T}_z + T''_z]$, $F_S = +D_s(R)[\bar{S}_z + S''_z]$, and their vertical convergences are given by

$$\begin{aligned} +\frac{\partial F_T}{\partial z} &= k_T \frac{\partial}{\partial z}\left[Nu(\bar{R} + R'') \frac{\partial(\bar{T} + T'')}{\partial z}\right] \\ &= k_T Nu(\bar{R}) \frac{\partial^2 T''}{\partial z^2} + k_T \frac{\partial \bar{T}}{\partial z}\frac{\partial Nu}{\partial \bar{R}}\frac{\partial}{\partial z}\left(\frac{\bar{T}_z + T''_z}{\bar{S}_z + S''} - \frac{\bar{T}_z}{\bar{S}_z}\right) \\ &= D\frac{\partial^2 T''}{\partial z^2} + D\bar{T}_z r_T \frac{\partial^2}{\partial z^2}\left(\frac{T''}{\bar{T}_z} - \frac{S''}{\bar{S}_z}\right), \end{aligned} \tag{5.2a}$$

$$+\frac{\partial F_S}{\partial z} = \frac{k_T}{\gamma}\frac{\partial}{\partial z}\left[RNu \frac{\partial(\bar{S} + S'')}{dz}\right] = \frac{D\bar{R}}{\gamma}\frac{\partial^2 S''}{\partial z^2} + \frac{D}{\gamma}\bar{T}_z r_S \frac{\partial^2}{\partial z^2}\left(\frac{T''}{\bar{T}_z} - \frac{S''}{\bar{S}_z}\right), \tag{5.2b}$$

where

$$r_T \equiv \frac{\bar{R}}{Nu}\frac{\partial Nu}{\partial \bar{R}},\ r_S = \frac{1}{Nu}\frac{\partial \bar{R} Nu}{\partial \bar{R}} = 1 + r_T, \tag{5.2c}$$

$$(r_T < 0)$$

and where the relatively small variation in the flux ratio γ (cf. Sections 3, 4) has been neglected.

For a 2D wave with streamfunction ψ'', and molecular viscosity ν, the vorticity equation is

$$\left(\frac{\partial}{\partial t} - \nu\nabla^2\right)\nabla^2\psi'' = +g\left(\frac{\partial T''}{\partial x} - \frac{\partial S''}{\partial x}\right). \tag{5.3a}$$

The heat/salt perturbation equations obtained using Eqs. (5.2) are

$$\bar{T}_z\psi''_x + \left(\frac{\partial}{\partial t} - D\frac{\partial^2}{\partial z^2}\right)T'' = Dr_T\frac{\partial^2}{\partial z^2}(T'' - S''\bar{R}), \tag{5.3b}$$

$$\bar{S}_z\psi''_x + \left(\frac{\partial}{\partial t} - \frac{D\bar{R}}{\gamma}\frac{\partial^2}{\partial z^2}\right)S'' = \frac{Dr_S}{\gamma}\frac{\partial^2}{\partial z^2}(T'' - S''\bar{R}). \tag{5.3c}$$

In solving the associated constant coefficient eigenfunction equations, it is now convenient to use a wave-dynamical nondimensionalization (rather than one related to the small-scale fingers in Section 2). Accordingly, let

$$z = Hz_1,\ x = Hk^{-1}x_1,\ t = [g(\bar{T}_z - \bar{S}_z)]^{-1/2}k^{-1}t_1, \tag{5.4a}$$

$$T'' = H\bar{T}_zT_1,\ S'' = H\bar{S}_zS_1,\ \psi'' = [g(\bar{T}_z - \bar{S}_z)]^{+1/2}H^2\psi_1, \tag{5.4b}$$

$$\epsilon_1 \equiv H^{-2}D[g(\bar{T}_z - \bar{S}_z)]^{-1/2},\ b \equiv \epsilon_1/k. \tag{5.4c}$$

In order to relate the following results to the more detailed numerics in the following section, we express the vertical wavelength $2\pi H$ as a multiple (Q) of the finger scale (d):

$$H \equiv Qd/2\pi \quad b = \frac{4\pi^2k_T^{-1}D}{Q^2k[Pr(1 - 1/R)]^{1/2}}. \tag{5.4d}$$

Since the parameter ϵ_1 is the ratio of a relatively small "eddy diffusion" rate (D/H^2) to the buoyancy frequency, we will be primarily interested in the case where $\epsilon_1 \ll 1$.

By introducing Eqs. (5.4) in Eqs. (5.3), simplifying, and then dropping "sub 1" we get

$$\left[\frac{\partial}{\partial t} - \frac{\nu b}{D}\left(\frac{\partial^2}{\partial z^2} + k^2\frac{\partial^2}{\partial x^2}\right)\right]\left(\frac{\partial^2}{\partial z^2} + k^2\frac{\partial^2}{\partial x^2}\right)\psi = +\frac{\partial}{\partial x}\frac{T\bar{T}_z - S\bar{S}_z}{\bar{T}_z - \bar{S}_z}$$

$$= +\frac{\partial T}{\partial x} + \frac{1}{\bar{R} - 1}\frac{\partial}{\partial x}(T - S), \tag{5.5}$$

$$\frac{\partial\psi}{\partial x} + \left\{\frac{\partial}{\partial t} - b\frac{\partial^2}{\partial z^2}\right\}T = br_T\frac{\partial^2}{\partial z^2}(T - S), \tag{5.6}$$

$$\frac{\partial\psi}{\partial x} + \left\{\frac{\partial}{\partial t} - \frac{\bar{R}b}{\gamma}\frac{\partial^2}{\partial z^2}\right\}S = r_S\frac{\bar{R}b}{\gamma}\frac{\partial^2}{\partial z^2}(T - S). \tag{5.7}$$

For the normal modes $(T, S, \psi) = (\hat{T}, \hat{S}, \hat{\psi})\exp(iz + ix)e^{\Omega t}$ Eqs. (5.5)–(5.6) become (respectively)

$$-\left[\Omega + \frac{\nu b}{D}(1 + k^2)\right](1 + k^2)\hat{\psi} = \left[\hat{T} + \frac{\hat{T} - \hat{S}}{\bar{R} - 1}\right]i, \tag{5.8}$$

$$\hat{\psi}i + (\Omega + b)\hat{T} = -br_T(\hat{T} - \hat{S}). \tag{5.9}$$

The third equation [obtained by subtracting Eqs. (5.6)–(5.7)] is

$$(\Omega + b)\hat{T} - \left(\Omega + \frac{\bar{R}b}{\gamma}\right)\hat{S} = -br_T(\hat{T} - \hat{S}) + \frac{\bar{R}br_s}{\gamma}(\hat{T} - \hat{S}),$$

or

$$(\hat{T} - \hat{S})\left[\Omega + b\left(r_T - \frac{\bar{R}r_S}{\gamma}\right) + \frac{\bar{R}b}{\gamma}\right] - b\left(\frac{\bar{R}}{\gamma} - 1\right)\hat{T} = 0. \tag{5.10}$$

When this is used to eliminate $\hat{T} - \hat{S}$ in (5.8) and (5.9) we get, respectively,

$$-\left[\Omega + \frac{\nu b}{D}(1 + k^2)\right](1 + k^2)\hat{\psi} = i\hat{T}\left[1 + \frac{b\left(\frac{\bar{R}}{\gamma} - 1\right)(\bar{R} - 1)^{-1}}{\Omega + b\left(r_T - \frac{r_S\bar{R}}{\gamma} + \frac{\bar{R}}{\gamma}\right)}\right],$$

and

$$-\hat{\psi}i = \hat{T}\left[\Omega + b + \frac{b^2\left(\frac{\bar{R}}{\gamma} - 1\right)r_T}{\Omega + b\left(r_T - \frac{r_S\bar{R}}{\gamma} + \frac{\bar{R}}{\gamma}\right)}\right].$$

By dividing the last two equations, we obtain a cubic equation for the growth rate Ω:

$$\left[\Omega + \frac{\nu b}{D}(1 + k^2)\right]\left\{(\Omega + b)\left[\Omega + b\left(r_T - \frac{r_S\bar{R}}{\gamma} + \frac{\bar{R}}{\gamma}\right)\right] + b^2r_T\left(\frac{\bar{R}}{\gamma} - 1\right)\right\}$$
$$= -\frac{\Omega}{1 + k^2} - \frac{b}{1 + k^2}\left(r_T - \frac{r_S\bar{R}}{\gamma} + \frac{\bar{R}}{\gamma} + \frac{\frac{\bar{R}}{\gamma} - 1}{\bar{R} - 1}\right).$$

Since $r_S = 1 + r_T$, this cubic simplifies to

$$\Omega^3 + a_2\Omega^2 + a_1\Omega + a_0 = 0, \tag{5.11a}$$

$$a_2 = \frac{\nu b(1 + k^2)}{D} + b\left[1 + r_T\left(1 - \frac{\bar{R}}{\gamma}\right)\right], \tag{5.11b}$$

$$a_1 = \frac{1}{1 + k^2} + b^2\left[1 + r_T\left(1 - \frac{\bar{R}}{\gamma}\right)\right]\frac{\nu}{D}(1 + k^2), \tag{5.11c}$$

$$a_0 = -\frac{b}{1 + k^2}\left[r_T - \frac{1}{\bar{R} - 1}\right]\left(\frac{\bar{R}}{\gamma} - 1\right). \tag{5.11d}$$

To leading order in $b \ll 1$ (cf. 5.4c) $a_2 \to 0$, $a_0 \to 0$, $a_1 \to (1 + k^2)^{-1}$, and therefore $\Omega = (-a_1)^{1/2} = \pm i(1 + k^2)^{-1/2}$ corresponds to nearly "pure" internal gravity waves.

The condition for their marginal stability, obtained by setting $\Omega = i\omega$ with ω real in (5.11), is $\omega^2 = a_1$, $a_2\omega^2 = a_0$, or

$$a_2 a_1 = a_0. \tag{5.12}$$

{If there are (as subsequently verified) two complex conjugate Ω roots, then the third root is $-b[(R-1)^{-1} - r_T][R/\gamma - 1] < 0$; this is damped because: Nu increases as $\bar{R}$ decreases, $r_T \leq 0$, and $\bar{R}/\gamma > 1$.} When (5.11b,c,d) is substituted in (5.12) we get

$$\left\{\frac{\nu}{D}(1+k^2) + 1 + r_T\left(1 - \frac{\bar{R}}{\gamma}\right)\right\}\left\{\frac{1}{1+k^2} + b^2\left[1 + r_T\left(1 - \frac{\bar{R}}{\gamma}\right)\right]\frac{\nu}{D}(1+k^2)\right\}$$
$$= -\frac{\frac{\bar{R}}{\gamma} - 1}{1+k^2}\left(r_T - \frac{1}{\bar{R}-1}\right)$$

or

$$\frac{\frac{\nu}{D}(1+k^2)+1}{1+k^2} = \frac{\left(\frac{\bar{R}}{\gamma} - 1\right)\Big/(\bar{R}-1)}{1+k^2} - b^2\left[1 - r_T\left(\frac{\bar{R}}{\gamma} - 1\right)\right]^2 \frac{\nu}{D}(1+k^2)$$
$$- b^2\left[1 - r_T\left(\frac{\bar{R}}{\gamma} - 1\right)\right]\left(\frac{\nu}{D}\right)^2 (1+k^2)^2. \tag{5.13}$$

Since $r_T \leq 0$ and $\bar{R}/\gamma > 1$, both b^2 terms are negative, so that a *necessary* condition for marginal instability is

$$\frac{\nu}{D} \leq \left(\frac{(\bar{R}/\gamma) - 1}{(\bar{R}-1)} - 1\right)(1+k^2)^{-1} = \left(\frac{(1/\gamma) - 1}{1 - 1/\bar{R}}\right)(1+k^2)^{-1},$$

or

$$A \equiv \frac{D}{\nu}\frac{\left(\frac{F_S}{F_T} - 1\right)}{\left(1 - \frac{\bar{S}_z}{\bar{T}_z}\right)} = \frac{F_S - F_T}{\nu(\bar{T}_z - \bar{S}_z)} \geq 1 + k^2 > 1. \tag{5.14}$$

If $\epsilon_1 \ll 1$ then $A > 1$ is also sufficient for instability, since k may be chosen such that $b^2 = \epsilon_1^2/k^2 \ll 1$ is negligible in (5.13). But if ϵ_1 is fixed and $k \to 0$, then $b^2 \to \infty$, and the right-hand side of (5.13) approaches *negative* infinity; this implies that ultra-long internal waves are not amplified. [Although the $A > 1$ condition for instability happens to be the same as in Stern (1969), the two theories are very different. The latter assumes that the wave shear rotates the local finger flux vector without changing its magnitude. Also

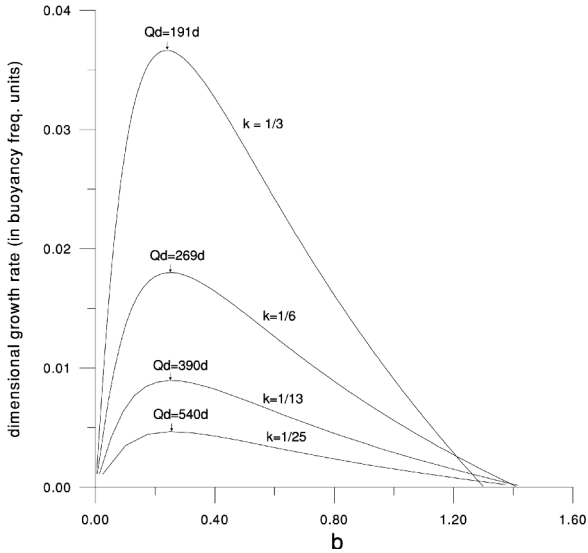

Figure 5. Solution of the cubic equation (5.11) for the growth rate for $Pr = 7$, $R = 1.25$, $\tau = 1/24$ as a function of k and H (see text). The values of $Nu = 86.7$, $\gamma = 0.68$, $A = 29$, $r_T = -3.12$ were obtained from a previous 2D numerical calculation (Fig. 3b).

different is Holyer's (1981) theory of the Floquet instability of *laminar* fingers with molecular diffusivities $k_T > k_S$.]

Typical growth rate curves (Fig. 5) relevant to heat-salt were obtained by solving the cubic for ($\tau = 1/24$, $Pr = 7$, $R = 1.25$) using the 2D values (Fig. 3b) of $Nu = 86.7$, $\gamma = 0.68$, $r_T = -3.12$; from these we get $A = 29.0$, $\nu/D = A^{-1}[1/\gamma - 1](1 - 1/R)^{-1}$. The value of b (Eq. 5.4d), obtained for various k and nondimensional wavelengths Q was plotted (Fig. 5) as a function of the growth rate (expressed as a fraction of the buoyancy frequency). The value of the dimensional wavelength at the arrows in Figure 5 is expressed in terms of the salt finger width (d) for $Nu = 86.7$. For a wave with $k = 1/6$ and $Q = 269d$ the growth rate is (0.02) times the buoyancy frequency, or (0.02/(1/6)) = 0.12 times the frequency of the amplifying k-wave. By way of illustration we note that for $d =$ 1 cm, the vertical half wavelength is $Qd/2 \sim 1.3$ meters, and the horizontal half-wavelength is $6 \times 1.3 = 7.8$ meters. It should be noted that the basic physical assumption of the parametric theory ceases to be valid if k is so large that the growth rate is comparable with the wave frequency, or if H/d is not large.

A physical explanation of the "overstable" oscillation can be obtained from Figure 6 which shows a plane internal gravity wave with velocity amplitude U'' inclined at a small angle (ϕ) to the horizontal. In the region of convergent vertical velocity (i.e., $\partial w''/\partial z < 0$), there is a vertical compaction (strain) of isotherms and isohalines (increased local $\partial T/\partial z$, $\partial S/\partial z$) which increases the downward finger fluxes. The convergence of the latter increases the mean density along the wave front in the region where the slanting velocity

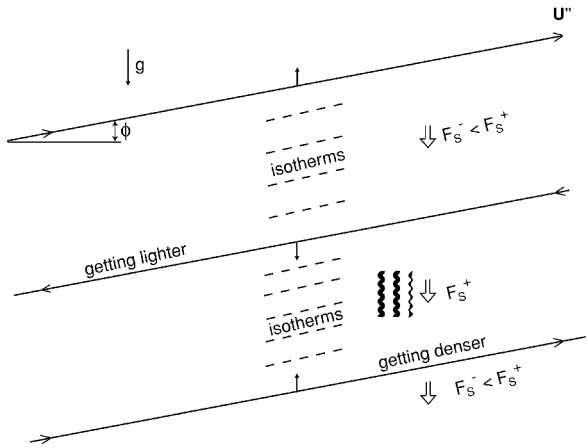

Figure 6. Illustrating the collective instability of a finite amplitude field of fingers (wiggly lines). The vertical component w'' of a large scale and slowly varying internal gravity wave with small amplitude U'' increases (decreases) the locally averaged $(\partial T/\partial z,\ \partial S/\partial z)$; the local salt flux $F_s^+ (F_S^-)$ is thereby increased (decreased), and the vertical divergences of these produce buoyancy perturbations in the scale of the wave. This amplifies if $A > 1$ (see text).

(U'') is upward. When this motion reverses and the fluid parcel returns to its starting z it has greater density, and consequently the maximum amplitude of U'' increases with time in an "over-stable" mode.

A simplified version of the foregoing theory can be obtained by noting that as a first approximation (in ϵ) the normal mode is a pure internal wave with $T'' \cong \bar{R}S''$, suggesting that the terms on the right-hand side of 5.3b,c [i.e., containing r_T, r_S] are negligible compared to the terms on the left-hand side containing only D, [as may be verified by the exact algebra given above for $\epsilon_1 \ll k \ll 1$]. Then by transforming the dependent variables in the simplified Eqs. 5.3b–c one can obtain a purely *formal* analogy with the well-known problem of the laminar diffusive instability of a stable salinity gradient which is heated from below (Baines and Gill, 1969), thereby immediately proving the instability. An interesting dividend emerging from this simplification is the value of the average wave flux ratio:

$$\gamma_W \equiv \frac{\langle \overline{\psi_x'' T''} \rangle}{\langle \overline{\psi_x'' S''} \rangle}. \tag{5.15}$$

at marginal stability $[\partial/\partial t \langle (T')^2 \rangle = 0]$. If the simplified ($r_T = r_S = 0$) Eq. 5.3b is multiplied by T'' and averaged we get $\bar{T}_z \langle \overline{\psi_x T''} \rangle + D\langle (\partial T''/\partial z)^2 \rangle = 0$; likewise (5.3c) gives $\bar{S}_z \langle \overline{\psi_x S''} \rangle + D(\bar{R}/\gamma)\langle (\overline{\partial S''/\partial z^2}) \rangle = 0$. Since $\partial T''/\partial z'' \cong R\partial S''/\partial z''$ for the normal mode it follows that $\langle (\partial T''/\partial z)^2 \rangle / \langle (\partial S''/\partial z)^2 \rangle = \bar{R}^2 + \ldots$, and therefore $\bar{R}\gamma_W = (\gamma/\bar{R})\bar{R}^2$ or $\gamma_W = \gamma$. *The important effect of the salt fingers on an internal wave is to (slightly) modify the relative phases of its components.* A broad band of internal waves [such as is

generated in the ocean by other causes] can be projected on the (slightly different) collective instability modes, thereby implying an amplification of waves that may exist in the background of the fingers. Also noteworthy is the fact that if ($\bar{R}$, D, r_T) are taken as constant, then Eqs. (5.5)–(5.7) are valid for a *finite* amplitude *plane* wave since the non-linear terms vanish identically. But this result of our ensemble average theory does not necessarily hold for an individual realization (such as considered below) because the smaller scale fluctuations of the chaotic finger fluxes will force an entire spectrum of weak disturbances.

Although the instability of a pure finger field, and the subsequent generation of larger scales, has been realized in laboratory experiments (Linden, 1978), it has not been established that the mechanism is due to collective instability ($A > 1$).

6. Numerical test of collective instability

It is, therefore, desirable to provide a *direct* numerical calculation from Eqs. (1.1) to test the prediction (Section 5) that the strain-induced vertical (T-S) gradients in a relatively large-scale gravity wave can modulate the finger fluxes in a way which amplifies the wave. Whereas the theory of Section 5 started ($t = 0$) with a basic state of statistically steady and homogeneous fingers which is then perturbed by an infinitesimal amplitude wave, it is computationally convenient (and physically instructive), to reverse the procedure by starting ($t = 0$) with a state consisting of a particular small finite amplitude internal gravity wave, with much smaller computer noise to generate the fingers. The question then is whether this "designated" wave will increase in energy, or whether its shear will inhibit the finger flux. Since two greatly different scales are now involved, we must restrict the numerical calculations to a 2D finger model with computationally "accessible" values of (τ, R, Pr) [not corresponding exactly to any known substance]. The nondimensional number A [in (5.14)] which is relevant to the instability is the buoyancy flux divided by the product of the density gradient and the molecular viscosity, or

$$A = \frac{F_S - F_T}{\nu(\bar{T}_z - \bar{S}_z)} \equiv \frac{Nu}{Pr}\frac{(1/\gamma - 1)}{(1 - 1/R)}. \tag{6.1}$$

Our procedure is to first make small domain [$O(10)$ fingers] calculations to find parameters yielding $A > 1$, in which case we expect that in a *larger* computational domain an internal wave will be amplified by its interaction with the fingers. Such a small domain 2D calculation (not shown) for $R = 1.2$, $Pr = 7$, $\tau = 1/3$, using 8 pairs of fingers in a 256×256 grid yielded $Nu = 79 \pm 8$, $\gamma = 0.84$, with a highly supercritical $A = 12$. A similar calculation for $R = 1.3$, $Pr = 7$, $\tau = 1/3$ gave $Nu = 47 \pm 5$, $\gamma = 0.82$ with $A = 6.4$. From these two calculations the approximate value of the second relevant number (5.2a) is

$$r_T = RNu^{-1}\partial Nu/\partial R \simeq -4.7. \tag{6.2}$$

Therefore we proceeded to make a large domain calculation for

$$R = 1.2,\ Pr = 7,\ \tau = 1/3, \tag{6.3}$$

[anticipating on the basis of Sections 3 and 4 that the result will underestimate the instability for $\tau = 0.01$ (i.e., heat-salt)].

The vertical extent of the computational domain in terms of the finger width (d) used in nondimensionalizing Eq. (1.1), was $230d$; the horizontal extent was $6.4 \times 230d$, the F.G.W. was $11.5d$, and the grid size was (2048, 256). The large-scale initial disturbance consisted of a finite amplitude plane wave whose fronts had a slope 1/6.4 (relative to the horizon) and which propagated upwards as determined by the phase of a classical internal-gravity wave; the vertical wavelength was equal to the domain size, and the initial peak temperature amplitude was $2T_\mu = 12$. At $t > 0$ the small-scale computer noise resulted in finger fluxes (Fig. 7a) which increased rapidly at $t > 75$, and then equilibrated at values of $Nu = 70$, $\gamma = 70/84$ which are essentially the same as in the small domain calculation. Subsequently, the gravity wave maintains its frequency while increasing its amplitude exponentially (Fig. 7b). This can be expressed as a Richardson number (Ri), defined here as the squared value of the undisturbed buoyancy frequency $[g\alpha(\partial \bar{T}_*/\partial z_*)(1 - 1/R)]$ divided by the square of the modal amplitude of the wave shear. The dimensional value of the latter is $(k_T/d^2)[(2U_\mu)(2\pi Q^{-1})]$, where k_T/d^2 is the unit of shear appropriate to Eqs. (1.1), $2U_\mu$ is the nondimensional velocity amplitude of the wave, and Q [see Eq. 5.4d] is its non-dimensional wavelength. We found (not shown) that although the value of

$$Ri = \frac{Pr(1 - 1/R)}{16\pi^2 U_\mu^2 Q^{-2}}$$

in $0 < t < 200$ first increased [from $Ri = 10$, to $Ri = 20$], it then dropped to $Ri = 2.5$ at $t = 200$, but a minimum value (see below) was not yet reached. Figure 8 shows the tilted salt fingers at a relatively early time.

A confirmation of the wave amplification was obtained from a similar calculation using a different initial condition consisting of a standing *cellular* internal gravity wave, with nodal surfaces at the x-z boundaries of the domain. Although there is now a large temporal oscillation of the heat flux, the average ($50 < t < 250$) in Figure 9 is close to that for the previously considered plane wave. Figure 10 shows the finger structure (T) embedded in the cellular wave. Figure 11a shows the total wave energy, defined here as the average of $0.5[(u'')^2 + (w'')^2] + 0.5Pr(1 - 1/R)^{-1}(\rho'')^2$, with its components (quadratic amplitude) oscillating at *twice* the buoyancy frequency. The wave energy is still increasing at $t = 225$, and the minimum $Ri(1.09)$ in Figure 11b is approaching unity.

7. Overturning waves

In view of the large computational time already required, the following more expeditious numerical code was developed to determine the maximum value of the wave energy.

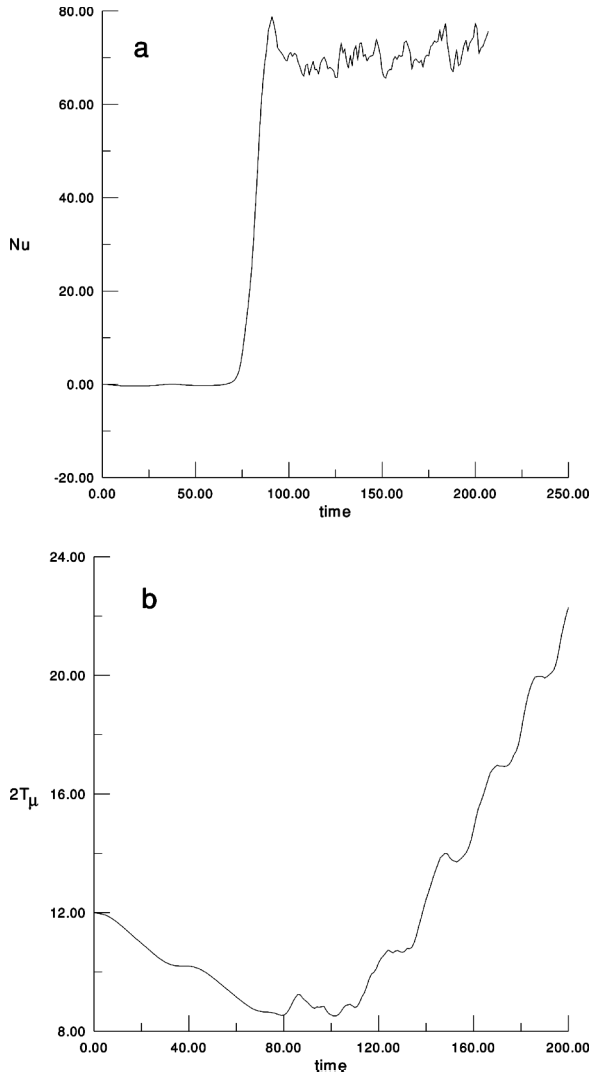

Figure 7. A test of the collective instability mechanism using a numerically "accessible" 2D model with $Pr = 7$, $R = 1.2$, $\tau = 1/3$ (see text) and a very large computational domain including 128 F.G.W. The initial disturbance consisted of a finite amplitude (plane) internal gravity wave with no fingers (except for computer noise). (a) The finger flux increases from $t = 0$ to an average $Nu = 70 \pm 3$. (b) The peak temperature amplitude of the initial wave also increases after the fingers develop, but T_μ has not yet equilibrated.

For this purpose we restrict attention to a *plane* wave whose fronts are inclined at a small angle ϕ to the horizon, and write Eqs. (2.1) in a "tilted box" (orthogonal) coordinate system whose x axis is also inclined at the angle ϕ. The gravity force then has an x as well as a z

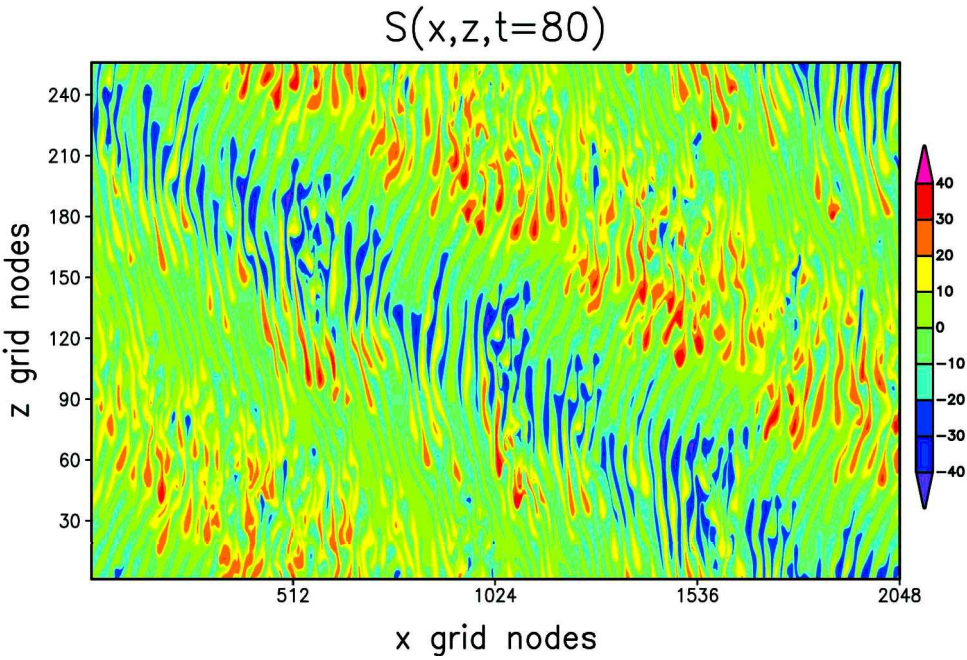

Figure 8. (a) A vertical salinity (S) section [for Fig. 7 at $t = 80$)] which reveals the fingers being tilted by the shear. The actual value of the total horizontal distance is 6.4 times larger than the total vertical distance.

component, and now the "designated" (initial) internal wave is denoted by x-wave number *zero*. The evolution of this is computed, along with the much smaller scale fingers, in a new (x, z) domain whose size [20 × 20 finger F.G.W.] is much less than that [128 × 20 finger wavelengths] in the vertical box model (Fig. 7). In the latter case the internal wave had nonzero wavenumber, which required the explicit computation of its (relatively unimportant) first, second, . . . harmonics; not all of these Fourier components are required or computed in the tilted box model, and consequently the computer time is reduced. Of course the smaller number of Fourier components in the tilted box model may result in a somewhat diminished quantitative accuracy, but the representation still allows for the collective instability mechanism. Although the Fourier series for **v**, T are now periodic in the coordinate system of the tilted box, the heat flux (Nu) given below is computed parallel to gravity by resolving **v** in that direction. The computations for $\phi = 1/6$ were performed by initializing the x-component of the upward propagating wave velocity as $U_\mu e^{i\mu z}$ + c.c., and the associated temperature deviations as $T_\mu e^{i\mu z} + c.c.$; these had exactly the same relative phase as in a classical internal wave. Although the amplitude $U_\mu(0) = 1.5$ was smaller than that used in Figure 7, the values of (τ, R, Pr) = (1/3, 1.2, 7) were the same, and small random computer noise was also used to initialize the fingers. After some testing of the spatial resolution Figure 12 was obtained using a 512 × 512 grid and a time step

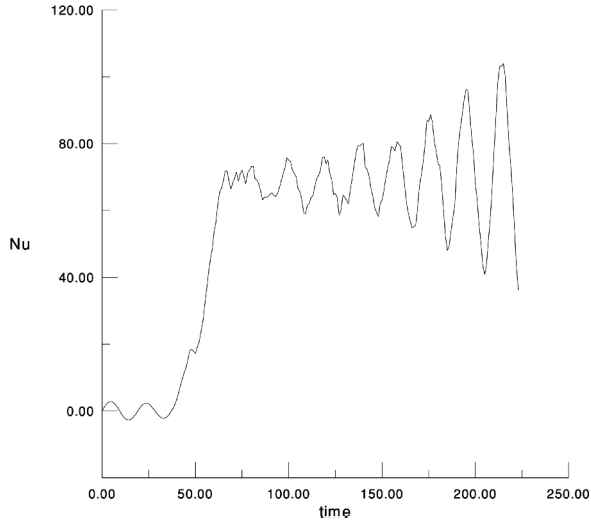

Figure 9. Same as Figure 8 except that the initial internal wave is standing *cellular* oscillation with horizontal and vertical nodal surfaces. Heat flux as a function of t. Note that the wave does not decrease the average finger flux.

$\Delta t = 0.005$ at $t = 0$. At $t = 50$ the flux levels off to a value $Nu = 80$. This is approximately 10% higher than the value in the vertical box (Fig. 7) (a difference which is attributed to the 50% smaller grid spacing (per F.G.W.) in the latter model) and approximately equal to that in a higher resolution small domain calculation.

The amplifying internal wave oscillations in Nu are clearly seen [Fig. 12] after $t = 180$, and the running mean Nu indicates that the *wave increases the average flux,* as predicted [Section 5]. The total kinetic plus potential energy (Fig. 13a) of the designated (largest scale) wave finally equilibrates at $t = 259$, and Figure 13c shows that a minimum Richardson number $\cong 0.5$ is reached at $t = 258$. Prior to this time an exponential fit (not shown) to the wave energy (Fig. 13a) gave a growth rate which was only 12% lower than the linear theoretical value $2\Omega = 2(0.0112)$ obtained from the cubic equation (5.11). Figure 13b shows that these calculations resolve the smallest scale in the salinity gradient; this is given by the spectrum of $\Sigma_m (k^2 + m^2)\hat{S}\hat{S}^*$ as a function of k (solid line), and by $\Sigma_k (k^2 + m^2)\hat{S}\hat{S}^*$ as a function of m.

Figure 14 gives the total kinetic energy in all the modes (a), as well as the integrated buoyancy work $(-\rho' w')$ term (b) and the total dissipation (c). The dashed-dot curve and the "x" points are reproductions of the respective solid curves, starting from $t = 260$, in which the time step has been reduced to $\Delta t = 0.0008$ (from $\Delta t = 0.001$). Although the two curves cease to track at $t = 279$, the $\Delta t = 0.0008$ calculation appears to be adequately resolved at $t \leq 281$, in view of the fact that the integrals in the equation for the rate of increase of kinetic energy balanced to an error which was 3% of the dissipation. The spike (sign reversal) in *total* heat flux at $t = 279$ in Figure 12 is due to an *upward*

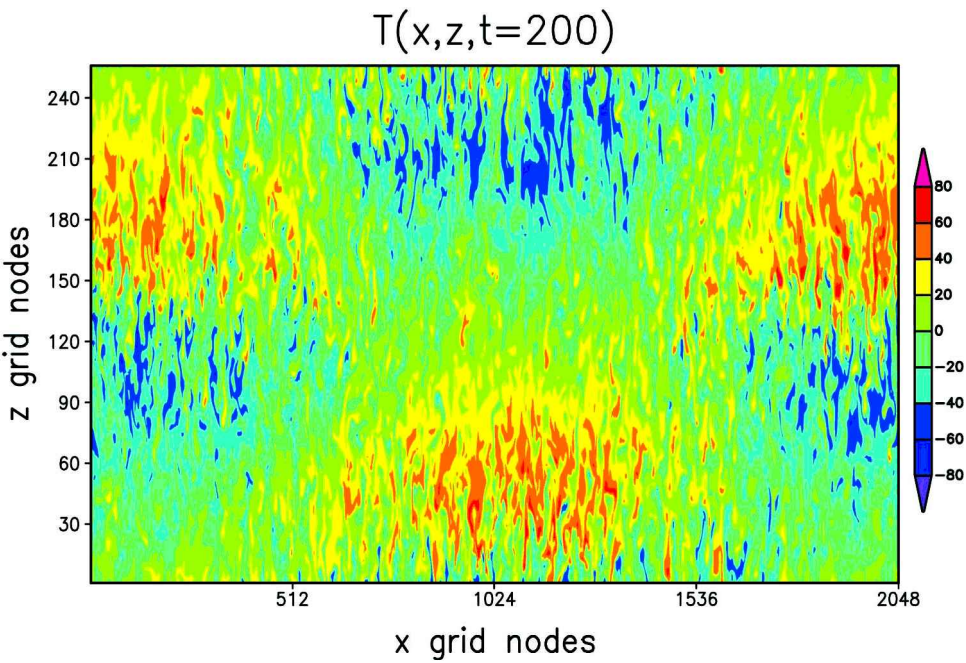

Figure 10. A vertical T section for Figure 9 revealing the fingers embedded in the cellular wave. Compare with the plane wave in Figure 8.

component (magnitude = 37.2) of the large-scale (>5 F.G.W.) wave in excess of the downward flux (25.6) of the fingers (<5 F.G.W.); the total downward salt flux, however, is positive. The points for the $\Delta t = 0.0008$ calculation (Fig. 14) confirm this spike, whose occurrence is consistent with the behavior of the low passed isopycnals (Fig. 15). These steepen at the earlier time (Fig. 15a), and in the subsequent (Fig. 15b) overturn the wave crest contains relatively cold and heavy fluid (originating at greater depths). The final result is a density inversion with sinking cold fluid, which accounts for the aforementioned *positive* wT of the large scale motion.

The calculation in Figure 15b was not continued in time because of the onset of a new kind of motion, viz., large Reynolds number convective "turbulence." In any further calculation the third dimension should be included and the domain size should also be increased (to get larger wavelengths). The resulting evolution should be similar to that which occurs with Kelvin-Helmholtz instabilities or critical layer absorption [Winters and D'Assaro, 1994] when the waves break. Such an effect in Figure 15b will probably "kill" the fingers, and the removal of this prime energy source tends to dissipate the larger scale motion. Later on however, the fingers should be re-established in the relatively quiet region, and so it goes. Patches of relatively large dissipation should appear intermittently [without necessarily forming a permanent "staircase"] after the fingers supply enough energy for the wave to overturn.

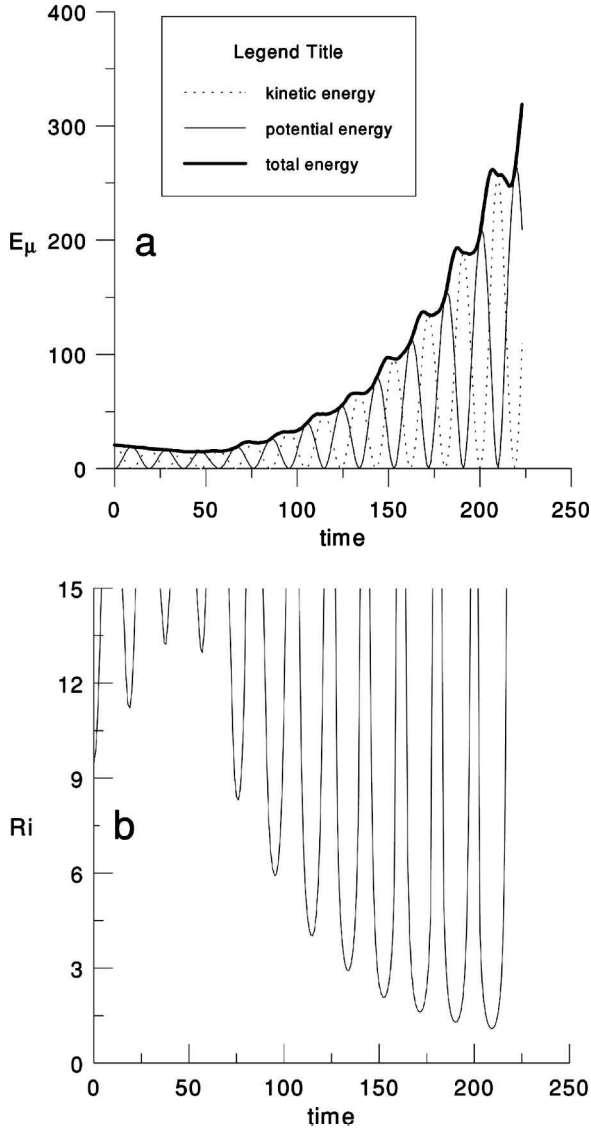

Figure 11. (a) The total wave energy and its two components for Figure 9. (b) Note that the minimum Richardson number has not yet been reached.

A similar tilted box calculation was made with an increased $R = 1.4$, for which we computed $Nu = 30.4 \pm 1.6$ ($\gamma = 0.83 \pm 0.01$, $r_T = -6.8$); these values produced a smaller $A = 3.1$, and a much larger e-folding time = 909. Consequently, a 50% larger initial amplitude of the "designated" (largest scale) plane wave was used in Figure 16, but this wave decays significantly *before* the finger flux reaches its equilibrium amplitude.

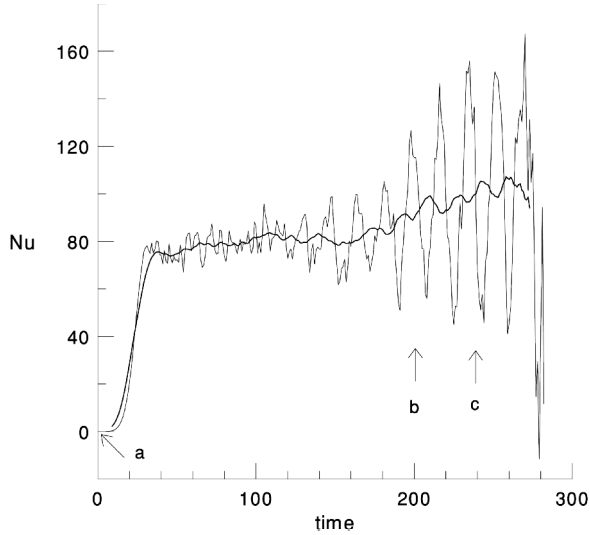

Figure 12. Time record of the total heat flux for $R = 1.2$, $\tau = 1/3$, $Pr = 7.0$ in the 20×20 F.G.W. tilted box model (see text). The heavy line is a running average (15 time units). The average total flux is increased by the presence of the wave! The arrows mark the beginning of the interval when, for the purpose of numerical stability, the time step was changed to: (a) $\Delta t = 0.005$, (b) $\Delta t = 0.002$, (c) $\Delta t = 0.001$. The spike at $t = 279$ with $-\langle \overline{wT} \rangle = Nu < 0$ corresponds to an upward heat flux (see text) in an overturning gravity wave.

Subsequently ($t \geq 80$) the internal wave amplitude stabilizes at a small finite value, with no *tendency* for *wavebreaking* even after a very long time. Although the two calculations (Figs. 15 and 16) confirm the theoretical result that finite amplitude internal waves can be maintained if $A > 1$, Figure 16 indicates that a higher critical value is required for wavebreaking. The latter effect might also depend on τ.

8. Conclusions and speculations

The 2D heat-salt ($Pr = 7$, $\tau = 0.01$) flux-gradient laws (Fig. 3b) in a "small" computational domain show that as the "overall" density ratio R decreases the fluxes and the eddy diffusivities [defined by the overall vertical gradients] increase substantially. These preliminary results may supply useful first approximations for finger fluxes in regions of the ocean thermocline where R varies on a vertical scale of a couple of meters.

Numerical calculations of the 3D-fluxes for $R = 2.0, 2.5$ were made and compared with the corresponding 2D-fluxes at the same τ, R. For $\tau = 1/6$ the ratio of (3D)/(2D) fluxes was approximately 2.0, and only slightly larger for $\tau = 1/12$. By extrapolating this ratio to $\tau = 0.01$, and by multiplying it with the directly calculated 2D flux at $R = 2.0$, we obtained first estimates [Eqs. 4.5] of the space-time average 3D fluxes for heat-salt fingers. The corresponding salt/heat diffusivities, are respectively $D_S = 0.24$ cm^2/sec and $D =$

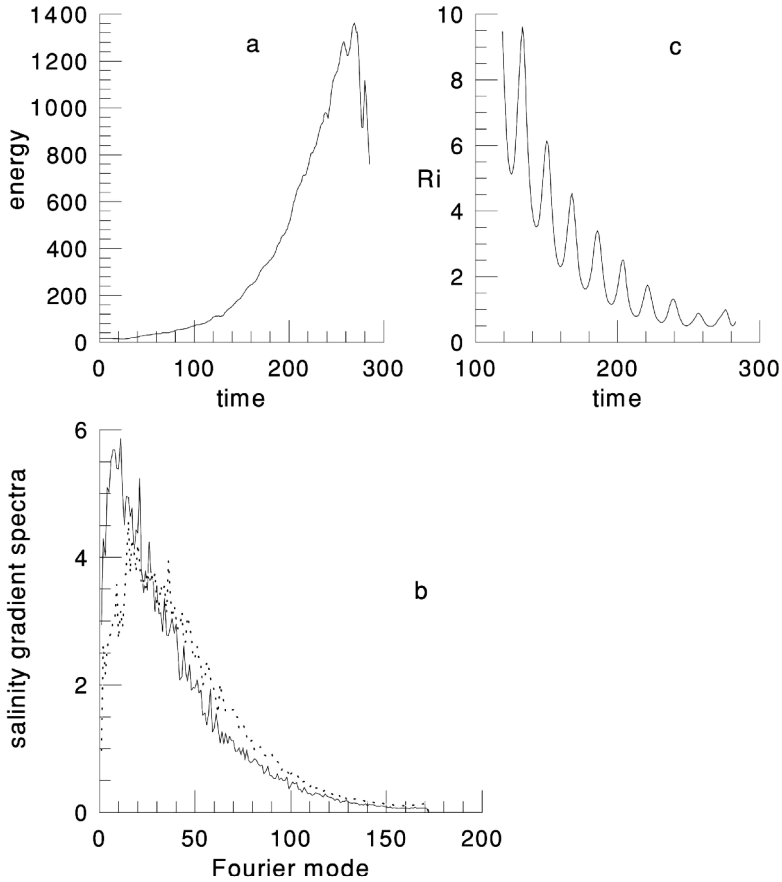

Figure 13. (a) Time record of the total internal wave energy which peaks at time $t = 259$. An exponential fit to the curve in $0 < t < 250$ gives a growth rate $2\Omega = 2(0.0098)$ which compares well with (5.11). (b) Salinity gradient spectra at $t = 248$; $\hat{S}(k, m)$ is the Fourier transform of S. $\Sigma_m (k^2 + m^2)\hat{S}\hat{S}^*$ (solid line) is shown as a function of k, and $\Sigma_k (k^2 + m^2)\hat{S}\hat{S}^*$ (dashed line) is shown as a function of m. The Fourier mode $k = 20$ corresponds to the fastest growing wave (F.G.W.). (c) Time record of the minimum Richardson number based on the maximum wave shear. This calculation resolves the least minimum Ri.

0.076 cm^2/sec. Also noteworthy is the result that at $\tau = 1/12$, $R = 2$ the anisotropy factor of fingers, as given by the ratio of the average $(\partial T/\partial z)^2$ to $(\nabla T)^2$, is approximately 0.18.

By using the results of Section 3 and 4 to parameterize the finger flux it was shown that if $A > 1$ the strain of an ambient internal wave field modulates the finger fluxes, thereby producing a slight phase shift in the components of the gravity wave. This results in a time average (downward) salt flux in the wave which exceeds the *wave* heat flux, and consequently the wave amplitude increases.

Perhaps the most important result is the direct numerical confirmation [Section 6] and

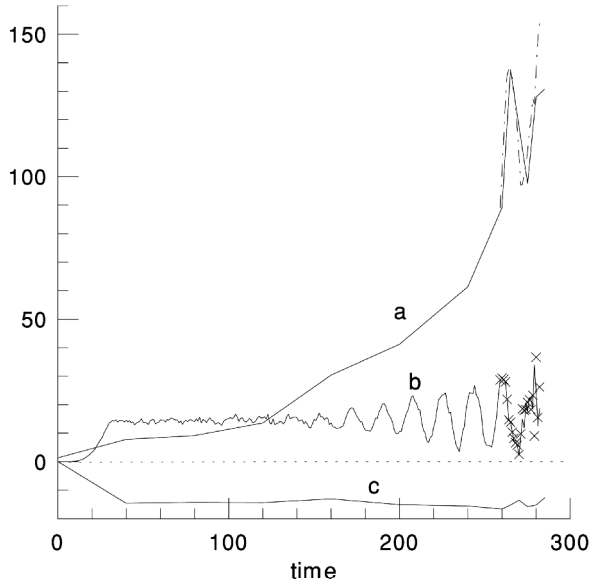

Figure 14. Energetics. (a) Time record of the total kinetic energy defined here as $\langle (u^2 + w^2)/2Pr \rangle$, (b) The rate of increase of total kinetic energy due to buoyancy (in the direction of gravity), (c) Viscous work $-\langle |\Delta\psi|^2 \rangle$. The "$x$" points and the "dashed dot curve" are reproductions of the run (solid curves) using a smaller time step $\Delta t = 0.0008$. See Figure 12.

elaboration of this effect in a model where both fingers and waves are resolved. The amplification of the wave shear does not decrease the finger flux [cf. Fig. 12] until the wave Richardson number drops to $Ri \sim 0.5$, at which point the tip of the isopycnals overturn (Fig. 15), producing large scale density inversions. We suggest that if the calculations were continued in time the accumulated wave energy would be rapidly dissipated in a more vigorous convective regime, similar to the 3D turbulence computed for mechanically driven wave overturns (Winters and D'Assaro, 1994). Our sample calculation of the fastest growing wave ($Qd/2 = 1.3$ meters) might be extended to estimate patch size due to finger instability.

Laboratory experiments (Linden, 1973) also show that a pure finger regime can give way to large scale eddies, and eventually these can form deep mixed layers separated by *thin* finger interfaces. In this regime (not discussed herein) the vertically averaged fluxes are much larger than in the pure finger (thick gradient) regime, and consequently the "small domain" 3D flux laws [Section 3 and 4] generally provide only lower bounds for the fluxes in the unbounded model with given overall gradients.

Since the salt field is the only prime energy source in our thermocline model, it does not tell us what the effect would be in an ocean which included the forces of the wind, tides, baroclinicity, etc. However, the calculation in Section 6 does contain some large scale shear effects with low Richardson number [$O(1)$]. Furthermore there are open ocean

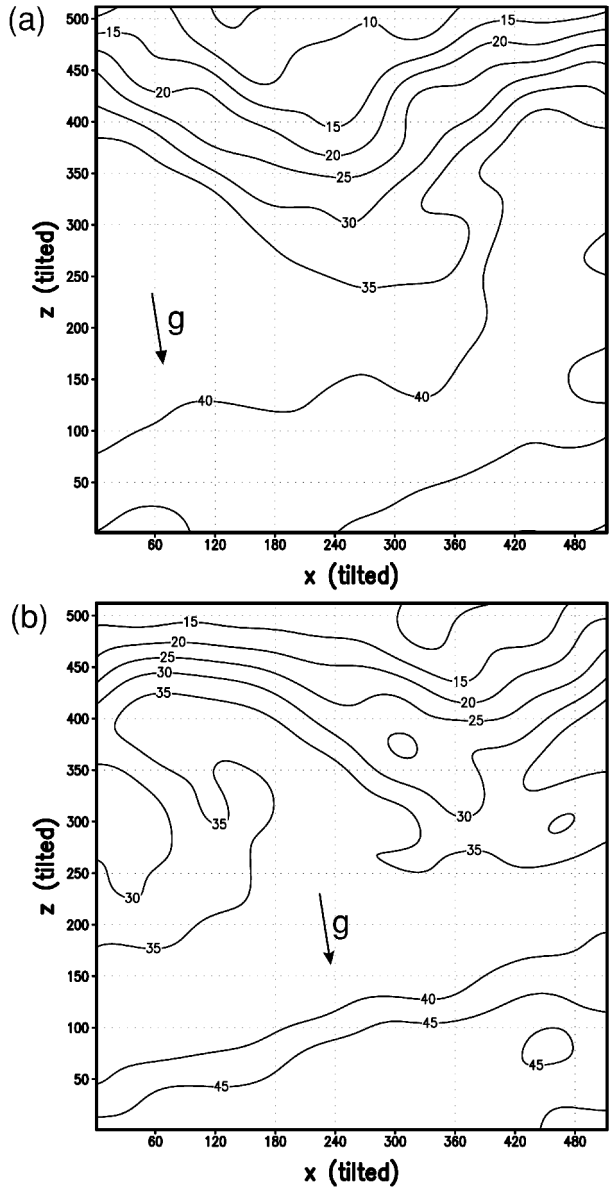

Figure 15. Total low passed density plots (nominal units) in the *tilted* (x, z) coordinate system (note the gravity vector); (a) at $t = 279$, (b) at $t = 281$. These show the steepening of the isopycnals, the onset of wave breaking and formation of density inversions. (The *actual* value of the average total density at $z = 512$ minus the average on $z = 1$ equals the undisturbed density difference measured parallel to the gravity vector g.) The axis are labeled in grid point numbers, and there is no vertical exaggeration.

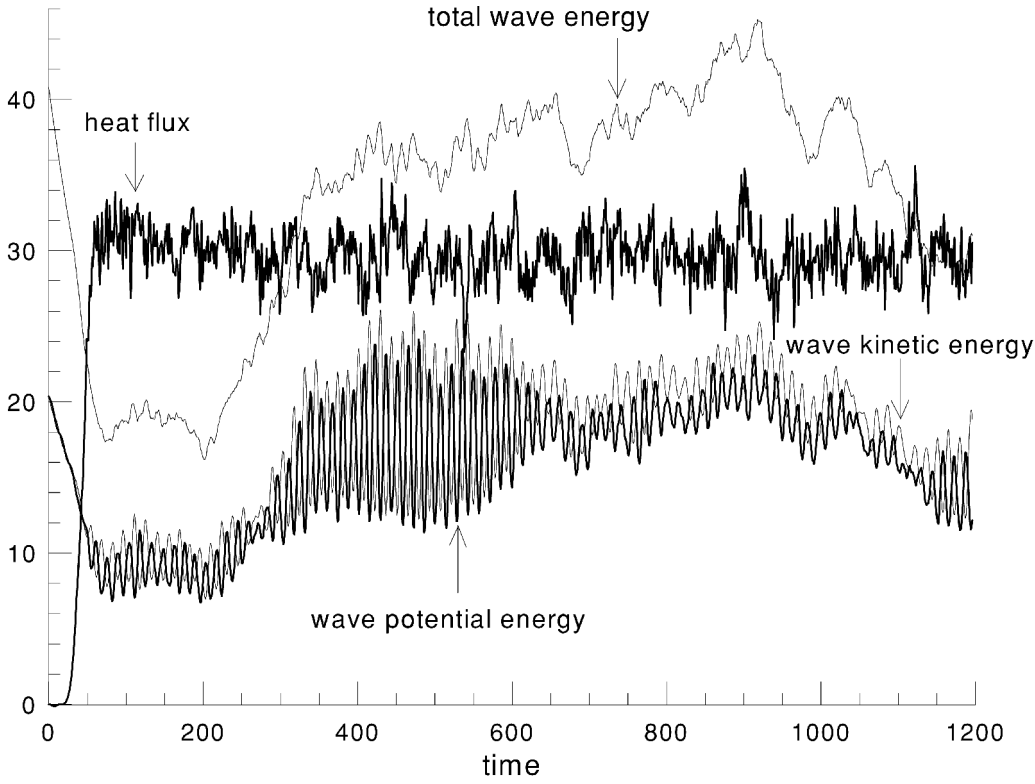

Figure 16. Same as Figure 12 except for a large $R = 1.4$, and a smaller $A = 3.1$. The energy in the designated wave (largest scale) is plotted.

regions where the effect of the aforementioned forces on the mixing in the main thermocline is minimal, and where comparison of microstructure measurements with our simple model might be instructive. In such an oceanic region (with $R < 2$) the horizontal tows of Mack (1985, 1989) reveal salt fingers in isolated patches (meter thick), but the fingers are unresolved in the much more extensive regions of the observations with $R \geq 2$; the calculations (Section 4) should be most applicable in these relatively "non-turbulent" regions. Mack also observed thin patches with "turbulent microstructure signatures," and these are also highly intermittent. The mechanism for producing these is conjectural, because overturning waves on a vertical scale of a couple of meters were virtually absent, in marked contrast with the abundance of overturns in shelf slope regions (Alford and Pinkel, 2000) where the strong tides and currents undoubtedly produce the turbulence. Despite their intermittency in the open ocean, the isolated turbulence patches have relatively large dissipation which makes a large contribution to the vertically averaged heat-salt fluxes, according to the microstructure soundings of Ruddick *et al.* (1997), St. Laurent and Schmitt (1999). The latter authors (in their Table 1) give D and D_S as a

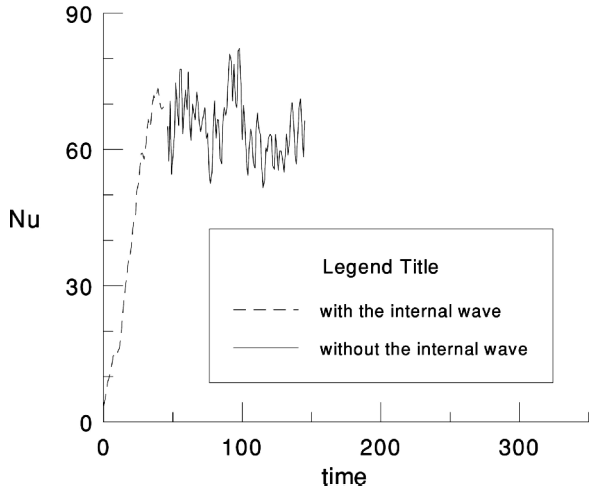

Figure 17. The effect of a horizontal shear flow $\bar{u}(z)$ [see Appendix] on the finger flux as a function of time. Also present at $t = 0$ was a finite amplitude internal wave, but it was removed at $t = 40$ and the size of the computational domain was reduced to eliminate collective instability. The $t > 40$ calculation shows that the finger flux was unaffected by $\bar{u}(z)$.

function of R; at $R = 2$ the measured (Cox Method) vertical temperature gradients yield $D = 0.07$ cm^2/sec. For regions with a smaller $R = 1.6$ St. Laurent and Schmitt (1999) obtain $D = 0.12$ cm^2/sec, and Ledwell *et al.* (1998) obtained similar values from observations of the vertical spread of a thin dye patch. In the smaller R regions the intermittent high dissipation patches in the soundings are most prominent. Although these might be due to "turbulence" of the Kelvin-Helmholtz type, we have suggested that a similar effect might be produced by fingers amplifying the background internal wave field in the ocean.

Acknowledgment. We gratefully acknowledge the financial support of the National Science Foundation. The School of Computational Science and Information Technology and the Academic Computing and Network Services of Florida State University kindly provided supercomputer time.

APPENDIX

The role of a horizontal shear flow and the finger Reynolds stress

As previously mentioned, the mechanism (Section 5) proposed for amplifying internal waves neglects the Reynolds stress which might be produced by the tilted fingers. To justify the neglect we took the output data at $t = 40$ in Figure 9 [which contained a finite amplitude internal wave as well as relatively weak fingers], and superimposed a purely horizontal shear flow $\bar{u}(z) = U_s \sin 2\pi z/Q$ whose amplitude $U_s = 8.0$ (or $Ri = 24$) was comparable to that in the internal wave. The subsequent evolution at $0 < t < 46$ as given in Figure 17 by the dashed curve, yields a final heat flux which is not much different from

what we previously got without (i.e., for $\bar{u} = 0$).

In order to examine the effect of a horizontal shear flow $\bar{u}$, in the absence of an internal wave oscillation, we then initiated a new run by removing from the data at $t = 46$ (Fig. 16) the longest vertical and horizontal wavelengths (i.e., the dominant internal wave), and reduced the size of the computational domain to 8×20 F.G.W. The subsequent evolution (the solid line in Fig. 17), containing only $\bar{u}$ and the 2D-fingers, shows that the purely horizontal shear flow (when it is weak enough) has very little effect on Nu. [The physical reason for this seems clear from the small vertical mixing length (λ) in Fig. 2c]. Furthermore, the subsequent evolution of the energy in $\bar{u}$ (not shown) is one of decay, in marked contrast to the previously found temporal increase in the internal waves. From these calculations we concluded that the finger Reynolds stress (not shown) is insignificant since its rate of work on $\bar{u}$ at $t > 150$ had a value $+0.031 \pm 0.03$ which was smaller than the work done by $\bar{u}$ against molecular viscosity. The plausible inference is that the finger Reynolds stress produced by a slightly *inclined* wave is negligible compared to the modified buoyancy forces.

REFERENCES

Alford, M. A. and R. Pinkel. 2000. Observations of overturning in the thermocline: The context of ocean mixing. J. Phys. Oceanogr., *30,* 805–832.

Baines, P. G. and A. E. Gill. 1969. On thermohaline convection with linear gradients. J. Fluid. Mech., *37,* 289–306.

Holyer, J. Y. 1981. On the collective instability of salt fingers. J. Fluid Mech., *110,* 195–207.

____ 1984. The stability of long, steady, two dimensional salt fingers. J. Fluid. Mech., *147,* 169–185.

Kelley, D. E. 1984. Effective diffusivities within oceanic thermocline staircases. J. Geophys. Res., *89*(C6), 10484–10488.

Kunze, E. 1987. Limits on growing, finite-length salt fingers: A Richardson number constraint. J. Mar. Res., *45,* 533–556.

____ 2001. A review of salt fingering theory. Prog. Oceanogr. (submitted).

Linden, P. F. 1973. On the structure of salt fingers. Deep-Sea Res., *20,* 325–340.

____ 1974. Salt fingers in a steady sheer flow. Geophys. Fluid Dyn., *6,* 1–27.

____ 1978. The formation of banded salt finger structure. J. Geophys. Res., *83,* 2902–2912.

Ledwell, J. R., A. J. Watson and C. S. Law. 1998. Mixing of a tracer released in the pycnocline of a subtropical gyre. J. Geophys. Res., *103,* 21,499–21,529.

Mack, S. A. 1985. Two-dimensional measurements of ocean microstructure: The role of double-diffusion. J. Phys. Oceanogr., *15,* 1581–1604.

____ 1989. Towed-chain measurements of ocean microstructure. J. Phys. Oceanogr., *19,* 1108–1129.

Radko, T. and M. E. Stern. 1999. Salt fingers in three dimensions. J. Mar. Res., *57,* 471–502.

____ 2000. Finite amplitude salt fingers in a vertically bounded layer. J. Fluid Mech., *410,* 1–28.

Ruddick, B., O. Phillips and J. Turner. 1999. A laboratory and quantitative model of finite-amplitude thermohaline intrusions. Dyn. Atmos. and Oceans, *30,* 71–99.

Ruddick, B., D. Walsh and N. Oakey. 1997. Variations in apparent mixing efficiency in the North Atlantic Central Water. J. Phys. Oceanogr., *27,* 2589–2605.

St. Laurent, L. and R. W. Schmitt. 1999. The contribution of salt fingers to vertical mixing in the North Atlantic Tracer Release Experiment. J. Phys. Oceanogr., *29,* 1404–1424.

Schmitt, R. W. 1981. Form of the temperature-salinity relationship in the central water: evidence for double diffusive mixing. J. Phys. Oceanogr., *11,* 1015–1026.

Shen, C. Y. 1995. Equilibrium salt-fingering convection. Phys. Fluids, *7,* 706–717.

Stern, M. E. 1969. Collective instability of salt fingers. J. Fluid Mech., *35,* 209–218.

Walsh, D. and B. Ruddick. 1995. An investigation of Kunze's salt finger flux laws. Are they stable? *in* Double Diffusive Convection. A. Brandt and H. J. S. Fernando, eds., AGU 195–211.

Winters, K. B. and E. A. D'Assaro. 1994. Three-dimensional instability near a critical layer. J. Fluid Mech., *272,* 255–284.

Received: *1 June, 2000;* revised: *30 April, 2001.*